

HST SNAPSHOT SURVEY OF POST-AGB OBJECTS

N. SIÓDIAK

Space Telescope Science Institute, 3700 San Martin Drive, Baltimore, MD 21218, USA and
 N. Copernicus Astronomical Center, Rabiańska 8, 87-100 Toruń, Poland

M. MEIXNER

Space Telescope Science Institute, 3700 San Martin Drive, Baltimore, MD 21218, USA

T. UETA

Department of Physics and Astronomy, University of Denver, 2112 E. Wesley Avenue, Denver, CO 80208, USA

B.E.K. SUGERMAN

Goucher College, 1021 Dulaney Valley Road, Baltimore, MD 21204, USA

G.C. VAN DE STEENE

Royal Observatory of Belgium, Ringlaan 3, 1180 Brussels, Belgium

AND

R. SZCZERBA

N. Copernicus Astronomical Center, Rabiańska 8, 87-100 Toruń, Poland

Draft version February 4, 2008

ABSTRACT

The results from a *Hubble Space Telescope* (*HST*) snapshot survey of post-AGB objects are shown. The aim of the survey is to complement existing *HST* images of PPN and to connect various types of nebulosities with physical and chemical properties of their central stars. Nebulosities are detected in 15 of 33 sources. Images and photometric and geometric measurements are presented. For sources with nebulosities we see a morphological bifurcation into two groups, DUPLEX and SOLE, as previous studies have found. We find further support to the previous results suggesting that this dichotomy is caused by a difference in optical thickness of the dust shell. The remaining 18 sources are classified as stellar post-AGB objects, because our observations indicate a lack of nebulosity. We show that some stellar sources may in fact be DUPLEX or SOLE based on their infrared colors. The cause of the differences among the groups are investigated. We discuss some evidence suggesting that high progenitor-mass AGB stars tend to become DUPLEX post-AGB objects. Intermediate progenitor-mass AGB stars tend to be SOLE post-AGB objects. Most of the stellar sources probably have low mass progenitors and do not seem to develop nebulosities during the post-AGB phase and therefore do not become planetary nebulae.

Subject headings: planetary nebulae: general — stars: AGB and post-AGB — stars: circumstellar matter — stars: mass loss — reflection nebulae

1. INTRODUCTION

The post-AGB¹ phase is a short period in the evolution of low- and intermediate-mass stars ($0.8 - 8M_{\odot}$) between the asymptotic giant branch (AGB) and the planetary nebula (PN) phases. The theoretical evolutionary tracks of the central stars (Blöcker 1995) predict that this phase lasts $10^2 - 10^5$ yrs, depending on the core mass, yet even

shorter kinematical age for nebulosities, of order of $10^3 - 10^4$ yrs (Sahai et al. 2007). Shorter kinematical life time is obvious from the observational point of view since the entire shell (especially an extended cold shell of post-AGB object) is not necessarily detected at the optical wavelength.

Many significant changes occur during this phase to both the star and the nebula. The superwind (suddenly increased mass loss at the end of the AGB phase) stops, large amplitude pulsations cease and the circumstellar envelope slowly expands and cools revealing the central star. The post-AGB star evolves at constant luminosity on the Hertzsprung-Russell diagram towards higher temperatures. The morphology of the expanding envelope changes, resulting in the fascinating shapes of the nebula itself.

Despite many efforts the post-AGB phase is still poorly understood. Especially the departure from spherically

Electronic address: siodmiak@stsci.edu, siodmiak@ncac.torun.pl
 Electronic address: meixner@stsci.edu
 Electronic address: tueta@du.edu
 Electronic address: ben.sugerman@goucher.edu
 Electronic address: gsteene@oma.be
 Electronic address: szczerba@ncac.torun.pl

¹ The term “proto-planetary nebulae” (PPN) is also often used to describe objects in transition between AGB and PN. However, one has to remember that low-mass objects that evolve very slowly will not be able to ionize the ejected matter and become planetary nebulae. Hence, the term “post-AGB” describes a wider group of evolved objects.

symmetric AGB circumstellar envelopes (e.g., Olofsson 2001) and the formation of diverse, axisymmetric, nebulae (e.g., Balick & Frank 2002) are of great interest to astronomers. Determining the main cause(s) of the breaking of mass-loss symmetry is an important issue in understanding the late stages of stellar evolution.

Previous morphological studies of post-AGB objects (e.g., Sahai et al. 1999; Kwok et al. 2000; Hrivnak, Kwok & Su 2000, 2001; Ueta, Meixner & Bobrowsky 2000, hereafter UMB00) revealed many asymmetrical nebulae around central stars, where jets and concentric arcs or rings were not unusual. Further, the ground-based mid-IR (8–21 μm) observations done by Meixner et al. (1999) showed two morphological classes of extended axisymmetric nebulae among post-AGB objects: “core/elliptical” with unresolved cores and elliptical nebulae and “toroidal” with limb-brightened peaks that suggest equatorial density enhancements.

Optical observations revealed more interesting details on structures seen in post-AGB nebulae. UMB00 observed 27 PPN candidates and divided them into two classes: the Star-Obvious Low-level Elongated (SOLE) nebulae which show star-dominated emission with faint extended nebulosity and DUST-Prominent Longitudinally EXTended (DUPLEX) nebulae which are dust dominated with a faint or completely obscured central star.

They also noticed that those two optical classes corresponded to the mid-IR ones, i.e. core/elliptical \approx DUPLEX and toroidal \approx SOLE, and that the main difference between SOLE and DUPLEX nebulae was the degree of the equatorial enhancement (i.e., DUPLEXes tend to have a higher equator-to-pole density ratio than SOLEs) and could not be attributed only to the inclination-angle effects. They also suggested that SOLE nebulae were optically thinner than DUPLEX nebulae and that SOLE PPNs would have evolved from low-mass progenitors and DUPLEX from high-mass progenitors. Later model calculations (Meixner et al. 2002) confirmed the physical differences between those two classes of objects. Other high-resolution near-infrared *HST* observations (e.g., Ueta, Murakawa & Meixner 2005; Su et al. 2003) also supported optical results. Follow-up studies by e.g., Ueta, Murakawa & Meixner (2005) were conducted to further investigate the asymmetry of observed objects. They also found that differences in observed morphologies are caused (mainly) by optical depth and (to a lesser extent) by inclination of the objects. All those observations strengthen the hypothesis of an equatorial mass loss enhancement at the end of the AGB (superwind) phase (Meixner et al. 1999) and that morphological shaping of nebulae occurs before the post-AGB phase. Moreover, the resulting diverse shapes observed in proto-planetary as well as PNs may be caused by some properties of the central stars such as chemical composition, mass and/or metallicity.

In order to find further support to those results we have executed an *HST* snapshot survey of post-AGB objects by increasing the range of masses and chemical composition (C/O ratio) and by enlarging the sample of studied objects. The goal of the project is to connect the observed diversity of nebular shapes with physical and chemical properties of the central stars. In this paper we present the results for post-AGB objects ob-

served recently with *HST*. Observation and data reduction are summarized in §2. The results and differences between selected groups of objects are shown in §3. In §4 we discuss obtained results with references to physical and chemical properties of stars. The conclusions are included in §5.

2. OBSERVATIONS

2.1. Sample selection

Post-AGB stars do not form a homogeneous group. One can find objects with different masses (including very low-mass objects that will never become PNs) and chemical composition. However, they are expected to be supergiants of spectral type B–K with an evidence of the circumstellar envelope (e.g., infrared excess) and no large photometric variability (the classification criteria for an object to be a post-AGB star were described in e.g., Kwok 1993; Van Winckel 2003; Waelkens & Waters 2004). In addition, few unique classes of stars like RV Tau objects (Jura 1986), R CrB stars and extreme helium stars (Renzini 1979; Iben et al. 1983) or even “born-again” supergiants (Sakurai’s object and FG Sge, e.g., Lawlor & MacDonald 2003) are considered as evolved objects in the post-AGB phase. All those objects are included in the Toruń catalogue of galactic post-AGB and related objects (Szczerba et al. 2007, <http://www.ncac.torun.pl/postagb>). From this database we selected for our snapshot survey² those sources that were not yet imaged with *HST*. Because the exposure time for an object from a snapshot survey cannot be too long, our sample was biased towards rather bright stars.

The selected post-AGB objects were observed with the High Resolution Channel (HRC) of the Advanced Camera for Surveys (ACS) on-board *HST* (Gonzaga et al. 2005), which has a $26'' \times 29''$ field of view and a plate-scale of $0.027'' \text{ pixel}^{-1}$. Observations for 19 objects from our proposal (program ID 10627, PI M. Meixner) were done between July 2005 and January 2007. We also searched for other post-AGB stars (from the Toruń catalogue) observed with ACS/HRC. In the *HST* Archive we found 17 objects from previous observation cycles. We included 14 post-AGB sources in our reduction and analysis of the images (selected objects from programs ID 9463 & 10185, PI R. Sahai and 9430, PI S. Trammell) and excluded 3 objects (the extended structures of Egg Nebula and Frosty Leo are bigger than the size of an image what prevents the correct measurements and IRAS 19024+0044 was already carefully analyzed by Sahai et al. (2005)). Together we have 33 PPNs observed in broad *B* (F435W), *V* (F606W) and *I* (F814W) filters. Selected candidates differ in central star masses, optical and infrared colors and effective temperatures (Stasińska et al. 2006, and references therein). Thereby we increased the number of studied post-AGB objects and covered more extensively the diverse nature of post-AGB stars. The properties of the analyzed post-AGB objects are shown in Table 1.

2.2. Data reduction and measurements

² Snapshot surveys are designed to fill the observational schedule gaps between larger GO programs and there is no guarantee that any particular snapshot target will be observed. That is why we may expect only part of the selected sample to be observed.

Table 1: Target summary for *HST* ACS/HRC observation of post-AGB objects

IRAS ID	Other name	Prop. ID ¹	V mag ²	J mag ²	T _{eff} ^{3,4}	Mass ⁴	C/O ⁴
01005+7910	...	10627	10.96	10.274	21000	0.55	C
04395+3601	AFGL 618	9430	...	13.510	25000 ^a	...	C ^a
06034+1354	DY Ori	10627	...	8.073	5900	< 0.55	O
08143-4406	PM 1-39	10627	...	9.172	7150	< 0.55	C
09256-6324	IW Car	10627	8.33	5.875	6700	< 0.55	C
11385-5517 ⁵	V885 Cen	9436	7.04	5.947	8500	0.55	O
12067-4508	RU Cen	10627	9.13	7.616	6000	< 0.55	O
12175-5338	V1024 Cen	10627	9.40	8.326	7350	0.62	O
12222-4652	HD 108015	10627	8.01	6.941	6800	< 0.55	O
12538-2611	LN Hya	10627	6.82	5.251	6000	< 0.55	O
13416-6243	...	10627	...	10.302	C ^b
13428-6232 ⁵	...	9463	...	13.176	C ^b
15039-4806	HD 133656	10627	7.58	6.680	8000	0.55	O
15469-5311	...	10627	10.82	7.190	7500	< 0.55	O
15553-5230 ⁵	...	10627	...	13.380
16206-5956	LS 3591	10627	10.00	9.002	8500	0.66	O
17163-3907	Hen 3-1379	10185	12.45	4.635
17243-4348	LR Sco	10627	10.49	8.035	6750	0.94	O
17279-1119	V340 Ser	10627	9.78	7.845	7300	< 0.55	C
17516-2525	...	9436	17.76	8.695	O ^b
17534+2603	89 Her	10627	5.51	4.998	6550	0.61	O
18135-1456	OH 15.7+0.8	9436	16.61	O ^c
19125+0343	BD+03 3950	10627	10.46	7.903	7750	0.58	O
19157-0247	BD-02 4931	10627	10.87	8.872	7750	0.58	O
19306+1407 ⁵	...	9436	...	11.286	B	...	O ^b
19475+3119 ⁵	HD 331319	9436	9.60	7.773	7750	0.58	O
20000+3239 ⁵	...	9436	...	8.021	5500 ^d	...	C ^b
20117+1634	R Sge	10627	9.31	7.818	5000	0.93	O
20547+0247	U Equ	9436	...	11.561	G	...	O ^e
22036+5306 ⁵	...	10185	...	11.666	O ^b
22223+4327 ⁵	BD+42 4388	9436	10.00	7.812	6500	0.55	C
23304+6147 ⁵	PM 2-47	9436	...	8.501	6750	0.66	C
23541+7031	M 2-56	9436	...	13.857	B	...	O ^b

¹ 9430 - PI S. Trammell, 9436 & 10185 - PI R.Sahai, 10627 - PI M. Meixner.² Magnitudes from GSC2.2 and 2MASS catalogues.³ Spectral type is shown if T_{eff} is not known from the model atmosphere analysis.⁴ Data collected by Stasińska et al. (2006) with few exceptions: ^a Cernicharo et al. (2001) and references therein, ^b C/O ratio established by the inspection of the ISO spectrum, ^c Engels (2002) and references therein, ^d Volk et al. (2002), ^e Geballe et al. (2005) and references therein.⁵ Images of those objects were also published in the newest paper by Sahai et al. (2007).

Each source was observed with various exposure times in order to increase the dynamic range of the final image. Faint nebulae were revealed in the long exposures, but the central star pixels were often saturated. The short exposures, free from saturated pixels, were combined with the longer ones to produce a nonsaturated final image. Because each object was observed a couple of times we had 2 or more nonsaturated final images. Then IRAF/STSDAS routines were used for calibration and reduction of images. The MultiDrizzle package was used to combine multiple frames of images into a single image (with plate-scale of 0.025'' pixel⁻¹), remove cosmic rays and subtract background radiation.

The reduced images were used to measure photometric and geometric properties of our objects. We adopted *HST* photometric calibration of SYNPHOT (v5.0, Laidler et al. 2005) to calibrate the flux density (F_λ in units of erg s⁻¹ cm⁻² Å⁻¹). The defined aperture was big enough to encircle the source together with the diffraction features, while the background emission was calculated from a (up to, depending on the proximity

of the other stars on the images) 10-pixel wide annulus separated from the selected aperture by a buffer zone. The sky emission was then subtracted from the emission of the entire source. The derived quantity, which was in counts per second, was finally converted into F_λ and *HST* ACS magnitudes (STMAG).

We measured the sizes of nebulosities around central stars. Our motivation was to determine the extension of the nebula as a whole, but not the sizes of its particular parts (e.g., each lobe). For this we needed only two axis of extension. In case of DUPLEX sources, where the central star was not visible and the lobes were clearly separated, we measured the size of each lobe separately and, in addition, the extension of the whole object. The extent of the nebula was defined to be the outermost recognizable structure in which emission level was from 1 σ up to 14 σ (depending on the image quality) above the background level. The major and minor axis, as well as the ellipticity of the nebulae were derived by fitting ellipses to the selected isophotes. We measured also surface intensity of the nebulae at the edge and compared it to the

Table 2: Properties of SOLE post-AGB objects

IRAS ID	Obs. Coord. (J2000)		ACS	F_λ^a	HST	I_s/I_n^c	Size	e^d
	ra	dec	filter		Mag ^b		(arcsec) (σ)	
01005+7910	01 04 45.59	79 26 47.08	F606W	1.23e-13	11.17	26900	3.75 x 2.20 (2)	0.41
			F814W	5.94e-14	11.97	14510	3.65 x 2.25 (4)	0.38
08143-4406	08 16 02.98	-44 16 04.88	F606W	5.58e-14	12.03	7500	2.10 x 1.30 (10)	0.38
			F814W	7.61e-14	11.70	3700	2.10 x 1.35 (4)	0.36
11385-5517	11 40 58.82	-55 34 25.52	F435W	8.10e-12	6.63	338000	8.30 x 6.60 (12)	0.20
			F606W	4.47e-12 ^e	7.27 ^e	81500	8.30 x 6.20 (8)	0.25
12175-5338	12 20 15.08	-53 55 31.62	F606W	6.46e-13	9.37	76000	5.70 x 2.50 (7)	0.56
			F814W	3.76e-13	9.96	36300	5.60 x 2.20 (10)	0.61
16206-5956	16 25 02.61	-60 03 31.35	F606W	3.33e-13	10.09	21500	3.85 x 2.60 (9)	0.32
			F814W	1.87e-13	10.72	21300	3.85 x 2.55 (6)	0.34
19306+1407	19 32 55.15	+14 13 36.89	F606W	7.83e-15	14.17	9000	7.70 x 2.00 (4)	0.74
			F814W	1.09e-14	13.81	6400	4.40 x 2.05 (4)	0.53
19475+3119	19 49 29.63	+31 27 15.32	F435W	6.91e-13	9.30	190000	10.45 x 5.10 (3)	0.51
			F606W	6.72e-13	9.33	153000	9.95 x 5.10 (2)	0.49
20000+3239	20 01 59.56	+32 47 33.71	F606W	3.39e-14	12.57	3800	2.15 x 1.45 (5)	0.33
			F814W	1.02e-13	11.38	2000	2.00 x 1.20 (7)	0.40
22223+4327	22 24 31.48	+43 43 10.67	F435W	3.47e-13	10.05	13000	3.40 x 2.10 (10)	0.38
			F606W	5.02e-13	9.65	10000	3.50 x 2.10 (6)	0.40
23304+6147	23 32 44.71	+62 03 48.92	F606W	3.30e-14	12.61	3800	2.25 x 1.60 (14)	0.29
			F814W	8.31e-14	11.60	2100	2.20 x 1.45 (9)	0.34

^a In units of $\text{erg s}^{-1} \text{cm}^{-2} \text{\AA}^{-1}$.^b HST system magnitudes (STMAG).^c Star surface intensity I_s to nebula surface intensity I_n ratio.^d Ellipticity $e = 1 - b/a$, where a and b are major- and minor-axis lengths, respectively.^e Due to a saturation problem, F_λ and HST Mag are only the lower limits.

Table 3: Properties of DUPLEX post-AGB objects

IRAS ID	Obs. Coord. (J2000)		ACS	F_λ^a	HST	I_s/I_n^c	Size	e^d
	ra	dec	filter		Mag ^b		(arcsec) (σ)	
04395+3601	04 42 53.50	+36 06 51.71	F606W	2.54e-15	15.39	...	15.40 x 4.80 (4)	0.67
		eastern lobe		1.98e-15	15.66	124	8.25 x 4.75 (4)	0.42
		western lobe		5.16e-16	17.12	85	6.20 x 3.20 (4)	0.48
13428-6232	13 46 20.96	-62 47 58.10 ^e	F606W
			F814W	3.86e-16	17.43	4	8.75 x 6.90 (1)	0.21
15553-5230	15 59 10.66	-52 38 38.15	F814W	1.90e-17	20.70	...	2.50 x 1.10 (2)	0.56
		eastern lobe		1.21e-17	21.20	10	1.35 x 1.00 (2)	0.26
		western lobe		6.01e-18	21.95	4	1.20 x 0.85 (2)	0.29
22036+5306	22 05 30.35	+53 21 33.97	F606W	1.32e-15	16.10	330	6.75 x 2.30 (3)	0.66
			F814W	2.87e-15	15.26	120	5.60 x 1.85 (4)	0.67
23541+7031	23 56 36.31	+70 48 18.39	F606W	5.33e-17	19.58	55	3.75 x 1.60 (2)	0.57
			F814W	4.96e-17	19.66	88	3.30 x 0.90 (1)	0.73

^a In units of $\text{erg s}^{-1} \text{cm}^{-2} \text{\AA}^{-1}$.^b HST system magnitudes (STMAG).^c Peak surface intensity I_s to nebula surface intensity I_n ratio.^d Ellipticity $e = 1 - b/a$, where a and b are major- and minor-axis lengths, respectively.^e 2MASS counterpart's coordinates. Only clearly visible part of the nebula was measured on F814W image (see text).

star (or peak if the central star was not visible, as in DUPLEX sources) surface intensity and got star-to-nebula surface intensity ratios (I_s/I_n). For objects without nebulae only the peak intensity was measured. Names and the coordinates of all objects, as well as other derived parameters (F_λ , HST magnitudes, I_s/I_n and extension) are shown in Tables 2, 3 and 4 for SOLE, DUPLEX and stellar sources, respectively.

Figures 1, 2 and 3 show the reduced images. The logarithmic scale is used to illustrate the contrast between nebulae and central stars. Nevertheless, some faint nebulae are still barely visible. I_s/I_n ranges from 4 to 3×10^5 (see Tables 2 and 3). The point spread function (PSF) ef-

fects are seen on most of the images. To remove them and to make the nebulae more clearly seen we deconvolved our images using Richardson-Lucy (RL) algorithm with a stellar PSF created especially for our images by the code TinyTim (v6.3, Krist & Hook 2004). As a result, the contrast between nebula and the background emission was improved in general, but in case of very faint nebulosities where the nebulae emission was comparable to sky emission, the difference between reduced and deconvolved images is rather insignificant. There is also one inconvenience in using RL algorithm, which is known to produce false depressions around unusually bright pixels. Those “holes” are seen on our deconvolved images, but

Table 4: Properties of stellar post-AGB objects

IRAS ID	Obs. Coord. (J2000)		ACS	F_λ^a	HST	I_s^c
	ra	dec	filter		Mag ^b	
12222–4652	12 24 53.49	–47 09 08.36	F606W	2.27e–12	8.01	1.28e+1
			F814W	1.21e–12	8.70	4.48e+0
12538–2611	12 56 30.00	–26 27 36.55	F606W	5.39e–12	7.07	1.21e+1
			F814W	4.08e–12	7.37	1.20e+1
13416–6243	13 45 07.26	–62 58 15.67	F814W	1.77e–15	15.78	6.47e–6
15039–4806	15 07 27.52	–48 17 53.85	F606W	3.11e–12	7.67	1.27e+1
			F814W	1.83e–12	8.25	6.34e+0
17163–3907	17 19 49.26	–39 10 38.29	F435W	7.93e–16	16.65	6.89e–3
			F606W	7.92e–14	11.65	4.38e–1
17279–1119	17 30 46.82	–11 22 08.21	F606W	5.47e–13	9.55	3.59e+0
			F814W	4.56e–13	9.75	5.27e+0
17516–2525	17 54 43.35	–25 26 28.77	F606W	5.35e–16	17.08	3.59e–3
17516–2525a ^d				4.39e–16	17.29	
17516–2525b ^d				6.12e–17	19.43	
			F814W	9.48e–15	13.96	3.24e–2
17516–2525a ^d				7.90e–15	14.16	
17516–2525b ^d				1.31e–16	18.61	
17534+2603	17 55 25.19	+26 03 01.49	F606W	2.07e–11 ^e	5.61 ^e	1.21e+1
			F814W	1.12e–11 ^e	6.28 ^e	1.23e+1
18135–1456	18 16 25.47	–14 55 16.17	F606W	5.56e–16	17.04	4.23e–3
			F814W	6.45e–16	16.88	3.37e–3
20547+0247	20 57 16.29	+02 58 44.47	F606W	3.85e–15 ^e	14.94 ^e	8.32e–3
			F814W	8.20e–15	14.12	2.35e–2
RV Tau stars:						
06034+1354	06 06 15.04	+13 54 18.95	F606W	7.67e–14	11.69	4.23e–1
			F814W	1.10e–13	11.30	3.25e–1
09256–6324	09 26 53.52	–63 37 48.78	F606W	1.45e–12	8.49	7.80e+0
			F814W	1.41e–12	8.53	5.27e+0
12067–4508	12 09 23.72	–45 25 34.60	F606W	6.02e–13	9.45	2.89e+0
			F814W	4.41e–13	9.79	1.93e+0
15469–5311	15 50 43.75	–53 20 42.88	F606W	2.64e–13	10.35	1.37e+0
			F814W	3.72e–13	9.97	1.23e+0
17243–4348	17 27 53.60	–43 50 46.73	F606W	2.46e–13	10.42	1.64e+0
			F814W	2.55e–13	10.38	1.07e+0
19125+0343	19 15 01.17	+03 48 43.52	F606W	2.71e–13	10.32	2.39e+0
			F814W	2.83e–13	10.27	1.24e+0
19157–0247	19 18 22.75	–02 42 10.79	F606W	1.93e–13	10.69	1.17e+0
			F814W	1.68e–13	10.84	6.11e–1
20117+1634	20 14 03.76	+16 43 35.77	F606W	9.79e–13	8.92	5.42e+0
			F814W	7.87e–13	9.16	3.04e+0

^a In units of $\text{erg s}^{-1} \text{cm}^{-2} \text{\AA}^{-1}$.

^b HST system magnitudes (STMAG).

^c Peak intensity (in units of $\text{erg s}^{-1} \text{cm}^{-2} \text{\AA}^{-1} \text{sr}^{-1}$).

^d See text for details.

^e Due to a saturation problem, F_λ and HST Mag are only the lower limits.

are not considered real structures. The deconvolved images are shown together with the reduced ones in Figures 1, 2 and 3 in the same logarithmic scale.

3. RESULTS

We detected nebulosities in 15 out of 33 sources and classified them as SOLE and DUPLEX following UMB00. SOLEs have an optically thin (continuous) envelope and the star is therefore very bright at optical and near-infrared wavelengths in comparison to the nebula (in terms of I_s/I_n we consider values of > 1000). The surface brightness peaks at the central star. Because of multi-axis lobes, with different shapes and surface brightness, UMB00 divided those objects in subgroups of simple ellipse, multiple ellipses, an ellipse with embedded bipolar structure and an ellipse with concentric shells. These structures are also present in our objects. In ad-

dition we observe snail-like structures. The PSF effects are apparent in the images: the faint nebular structures are often buried under the PSF of the bright central star. DUPLEXes have an optically thick torus that completely or partially obscures the central star. I_s/I_n values are much below 1000 and the peak of the surface brightness is far away from the center of the object. The nebula is bipolar and the (multiple) lobes are seen through scattered light. The PSF diffraction feature is usually not seen in the images of DUPLEX objects.

These observational characteristics of the nebulae are consistent with the present understanding of the structure of these shells, in which SOLE and DUPLEX nebulae respectively represent the low and high ends of the degree of equatorial enhancement for an intrinsically axisymmetric circumstellar shell. In other words, there is

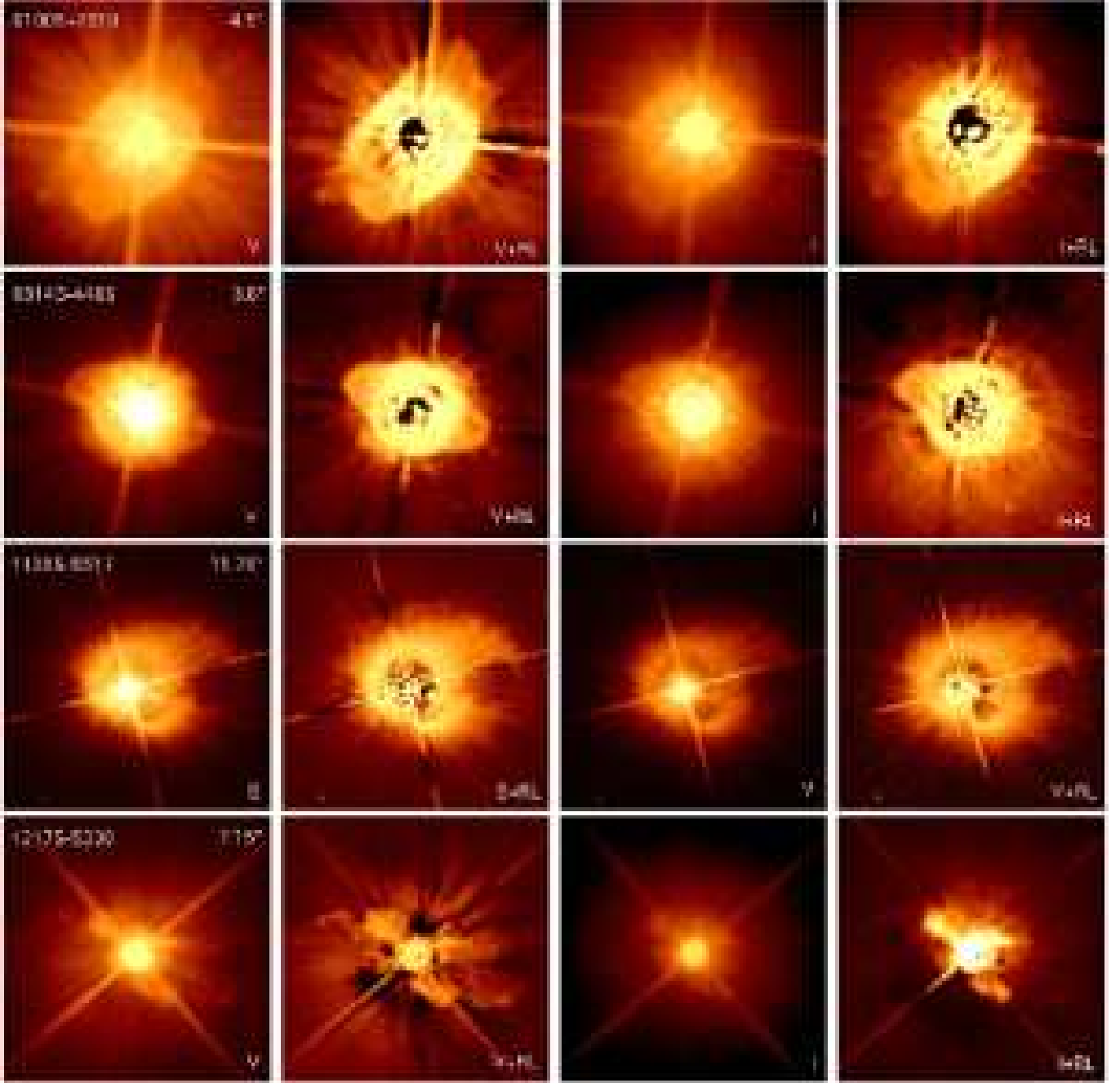


Fig.1. - Images of SOLE objects (north is up and east is to the left) shown in order of increasing RA (see Table 2). The leftmost frame shows the IRAS ID and size of an image. The filters types are shown at the bottom of each frame with “+RL” indicating Richardson-Lucy deconvolution. The images are in logarithmic scale to illustrate the contrast between central star and the nebula.

not much of a difference between SOLE and DUPLEX nebulae as far as the shell structure goes, but the difference is the optical depth along the equator due to the difference in the equator-to-pole density ratio resulting from the different degree of equatorial density enhancement. This is what makes DUPLEX nebulae appear bipolar with a well-defined dust lane, while making SOLE nebulae appear elliptical without a clear dust lane. Because of this, their shell morphology tends to become less definitive when the optical depth along the equator is close to unity (and/or the inclination angle of the shell is far from edge-on).

We have 10 SOLE objects (IRAS 01005+7910, IRAS

08143–4406, IRAS 11385–5517, IRAS 12175–5338, IRAS 16206–5956, IRAS 19306+1407, IRAS 19475+3119, IRAS 20000+3239, IRAS 22223+4327 and IRAS 23304+6147) and 5 DUPLEX objects (IRAS 04395+3601, IRAS 13428–6232, IRAS 15553–5230, IRAS 22036+5306 and IRAS 23541+7031) in our sample. I_s/I_n for our DUPLEXes is at most 330 (IRAS 22036+5306) and for SOLEs reaches the value of a few hundred thousands (e.g., IRAS 11385–5517 or IRAS 19475+3119). The remaining 18 sources do not show any nebulosities around them and are referred to as stellar objects. Due to a different morphology we may expect also the differences in spectral energy distribution

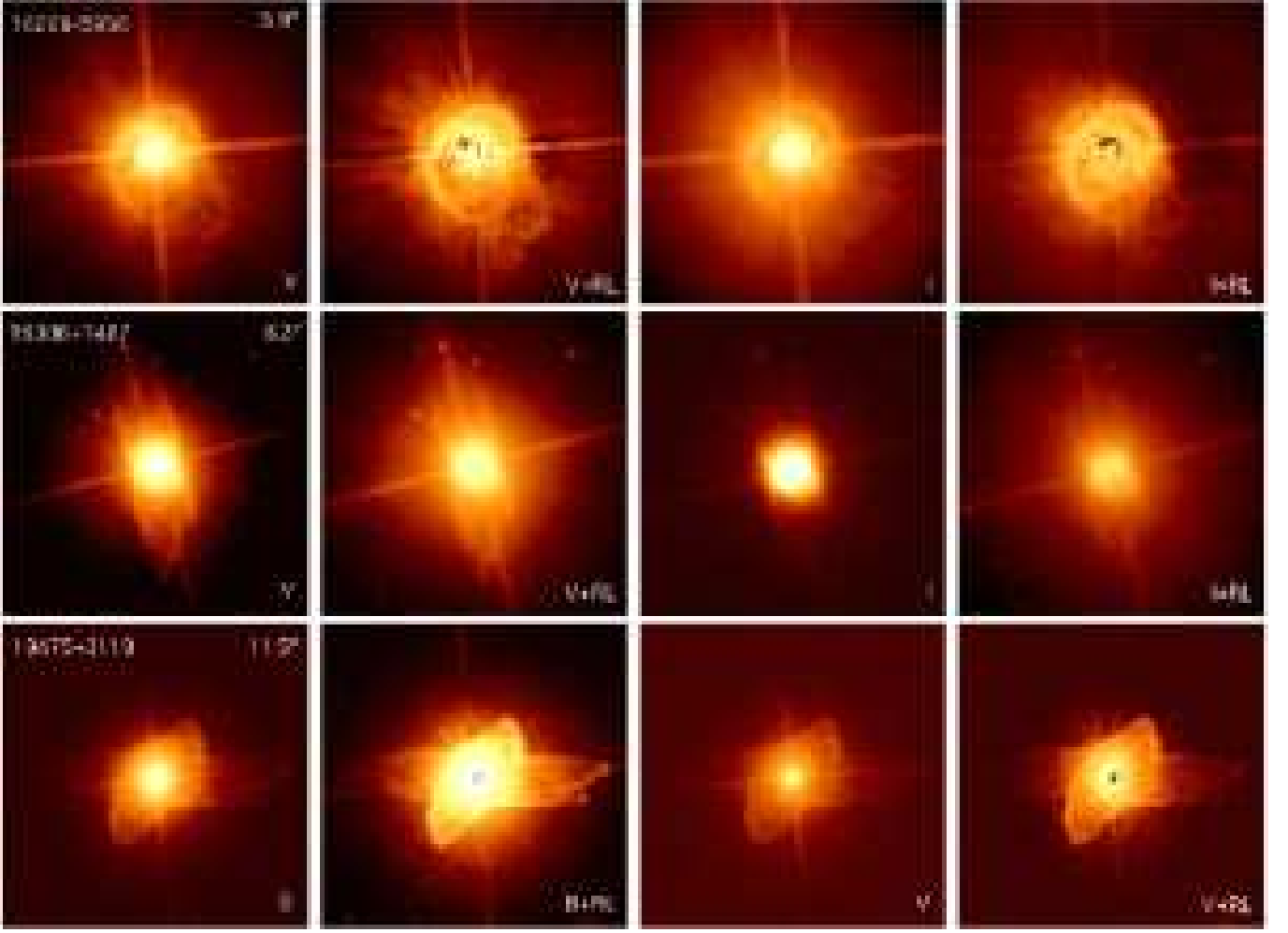


Fig.1. - continued.

(SED) shapes and the position in infrared color-color diagrams. All groups of sources are discussed separately in the following sections. Images of SOLE, DUPLEX and stellar objects are shown in Figures 1a, 1b and 1c, respectively.

3.1. SOLE objects

IRAS 01005+7910 have a nebulosity of the similar size in both bands ($3.75'' \times 2.20''$ in V and $3.65'' \times 2.25''$ in I). Its morphology is irregular. It has two lobes of different shapes pointed in north-west and south-east and additional small lobe emerging in south-eastern direction visible in the V band. The circular halo corresponds to the wings of the PSF around the bright central star.

IRAS 08143–4406 shows an elliptical nebula of $2.1''$ long and $1.4''$ wide. It has two small lobes emerging in western and eastern direction. The circular PSF halo is also present. The object looks similar in both bands with the only exception in I_s/I_n , which is two times bigger in the V band than in the I band. This source is a carbon-rich object with the overabundance of s-process elements (Reyniers et al. 2004) and is similar in appearance to IRAS 07430+1115 from UMB00 sample, which is also rich in s-process elements (e.g Reddy, Bakker & Hrivnak 1999).

The nebulosity of IRAS 11385–5517 is very asymmet-

ric and looks like pinwheel. This A-type oxygen-rich low-mass supergiant was thought to be a binary, but later observations suggested rather disk-like structure and high-velocity bipolar outflows (e.g., Olofsson & Nyman 1999). It is possible that we see only one of this outflows on *HST* images because of the inclination effect. The snail-like shape of the outflow is quite similar to the spiral pattern found in C-rich AGB star AFGL 3068 (Mauron & Huggins 2006). The spiral outflow in IRAS 11385–5517 is also single-armed and its extension is $8.3'' \times 6.6''$ in the B band. The object is very bright ($B=6.6\text{mag}$ and $V=7.3\text{mag}$) and looks similar in both bands. I_s/I_n is very high in the B band with the value of $\sim 3.4 \times 10^5$ being the highest among SOLE sources.

IRAS 12175–5338 has very complex morphology. The nebula is $5.7''$ long and $2.5''$ wide. It has at least 4 lobes, pointed in different directions. The lobes are of very different brightness, with the bright ones closer to the central star and very faint more extended structures. They are less clearly visible in the I band. The circular PSF halo is also seen around the star. The object is quite bright in both bands, $\sim 9.5\text{mag}$, and is known to be a metal-deficient pulsating variable (e.g., Van Winckel 1997).

IRAS 16206–5956 has a nebulosity very similar to the one seen in IRAS 11385–5517. It is also asymmetric and

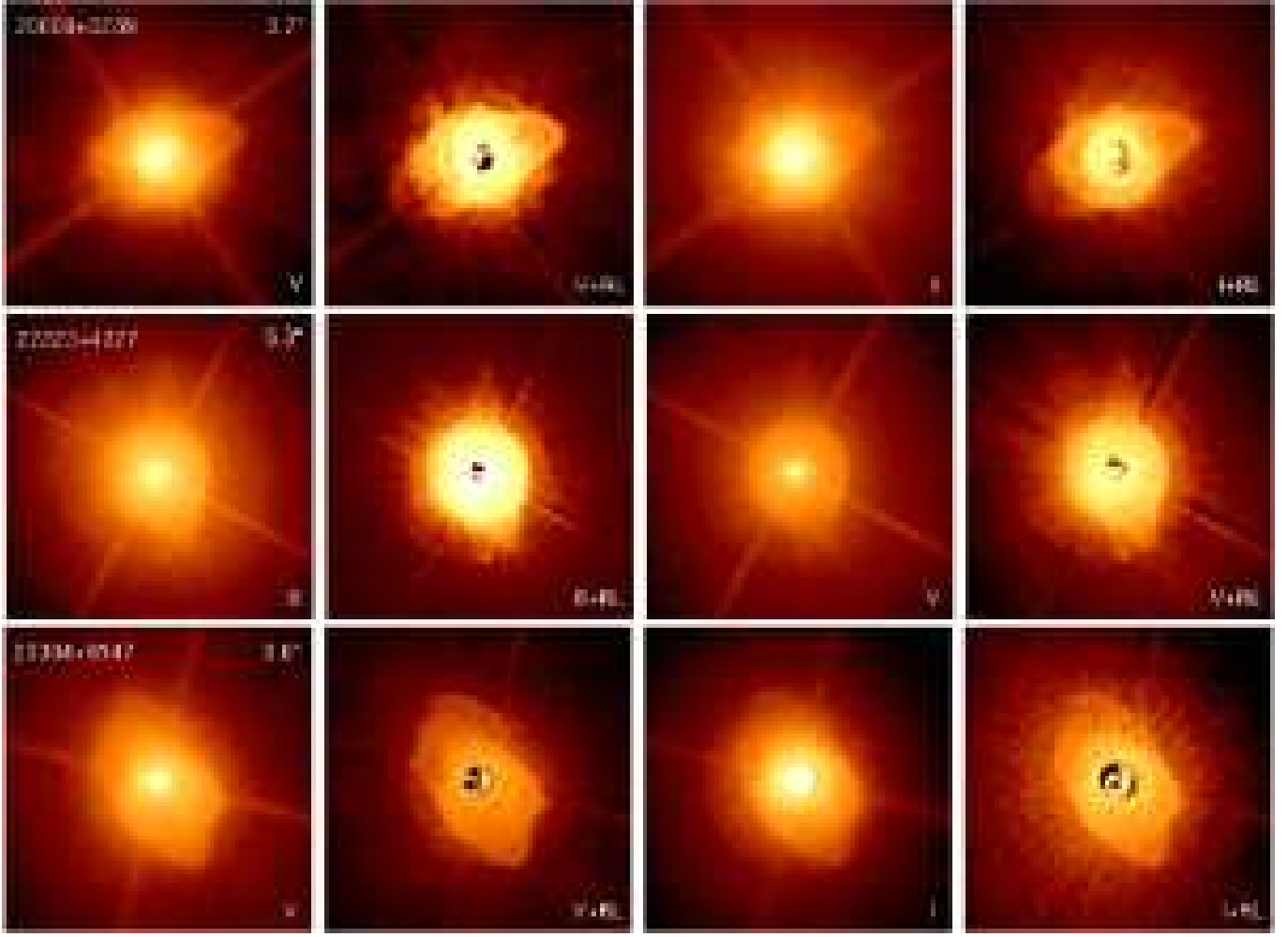


Fig.1. - continued.

has a snail-like shape, but is much smaller with an extension of $3.85'' \times 2.6''$. There is also a faint lobe emerging to the south-west with a quite complex structure. There is no visible lobe on the other side of the objects, but it may be extremely faint and buried under the PSF of the bright central star. The structures are better resolved in the V band than in the I band, but I_s/I_n is the same, ~ 21000 , in both bands. IRAS 16206–5956 is also A-type oxygen-rich supergiants similar to IRAS 11385–5517, but is more massive with a core mass of $M = 0.66M_\odot$ (see Table 1).

IRAS 19306+1407 is a B-type oxygen-rich PPN. It has a bright central star and low surface brightness lobes (I_s/I_n is ~ 9000 and 6400 in the V and I band, respectively). The lobes have bipolar structure, also seen in previous observations (Volk, Hrivnak & Kwok 2004; Sahai 2004). The lobes seem to be smaller in the I band, with the extension of only $4.4'' \times 2.0''$, in comparison to the V band where they are longer, $7.7'' \times 2.0''$.

IRAS 19475+3119 has a quadrupolar nebula and a PSF spherical halo. Similar complex double-elongation structure can be seen in IRAS 04296+3429 from UMB00, except for the different sizes of the nebula: IRAS 19475+3119 has much bigger nebulosity of $10.45''$ long and $5.1''$ wide. Also, IRAS 19475+3119 is known to be oxygen-rich (its dust envelope was described in details

by Sarkar & Sahai 2006), whereas IRAS 04296+3429 is a carbon-rich source with s-process overabundance and $21 \mu\text{m}$ emission feature (e.g., Volk, Kwok & Hrivnak 1999).

IRAS 20000+3239 is a carbon-rich source with s-process elements and $21 \mu\text{m}$ feature (e.g., Volk, Kwok & Hrivnak 1999; Van Winckel & Reyniers 2000). It has small lobes emerging to west and east with the extension of $2.15'' \times 1.45''$ in V (and slightly smaller in I band) and is very similar to IRAS 08143–4406 described above.

IRAS 22223+4327 is also a carbon-rich source with s-process elements and $21 \mu\text{m}$ feature. It is quite bright in V band (~ 9.6) and the nebula has a size of $3.4'' \times 2.1''$. There are two pairs of lobes pointed to north and south and they are more clearly visible on the south side. The object is quite similar to IRAS 08143–4406 and IRAS 20000+3239.

IRAS 23304+6147 also belongs to the group of objects with $21 \mu\text{m}$ feature. Its extension is comparable to the extension of IRAS 20000+3239 ($2.25'' \times 1.6''$). It has 2 lobes emerging in northern and southern directions and another inner pair of lobes in western and eastern directions. Those inner lobes are not so clearly seen even on deconvolved images. The object's structure could be similar to one seen in IRAS 06530–0213 from UMB00. While the appearance of IRAS 20000+3239,

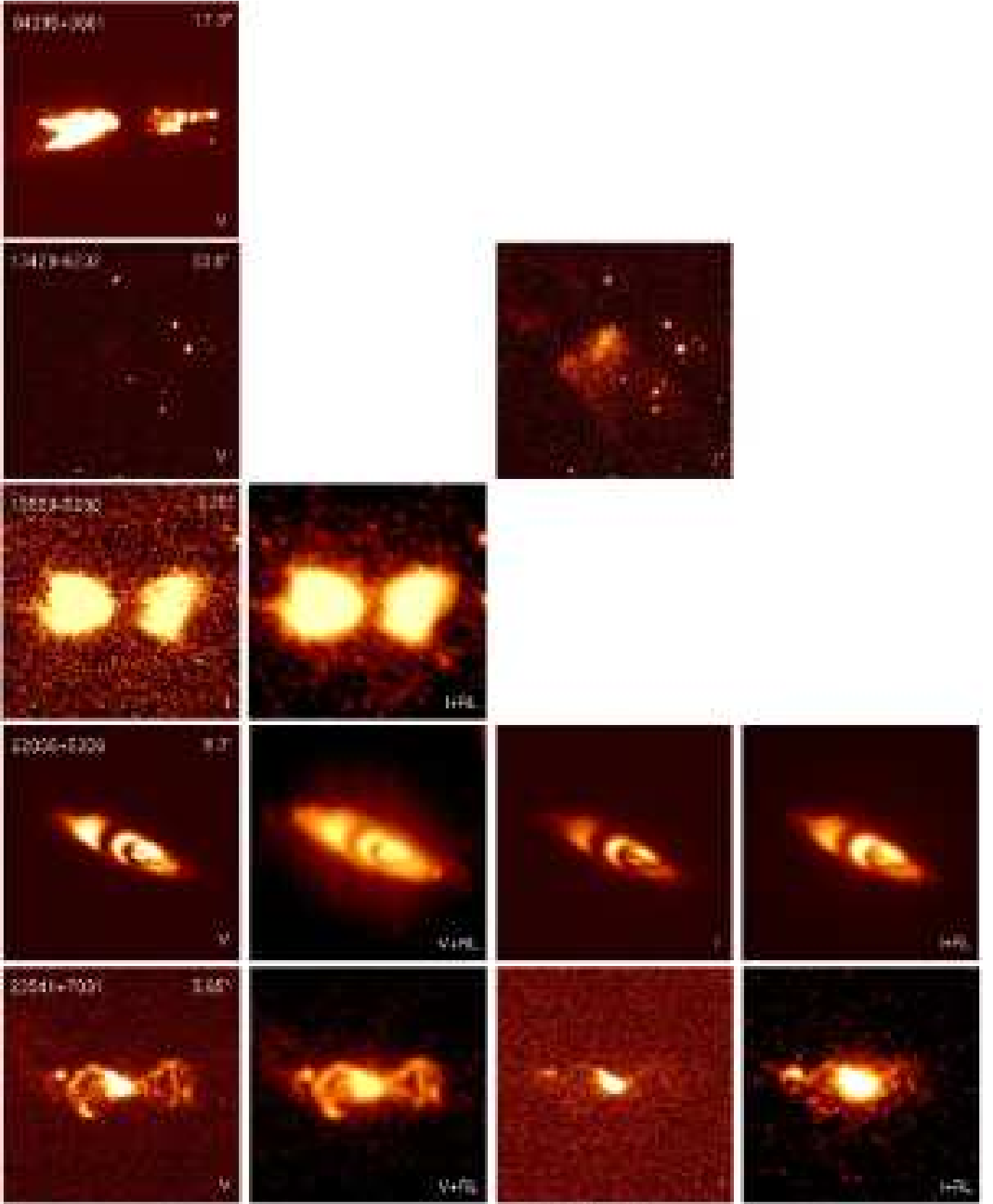


Fig.2. - Images of DUPLEX objects shown in order of increasing RA (see Table 3). The displaying scheme is the same as in Fig.1.

IRAS 22223+4327 and IRAS 23304+6147 is similar and those three objects have the same $21 \mu\text{m}$ feature, the SOLE morphology is not characteristic to the

whole group with $21 \mu\text{m}$, e.g., DUPLEX source IRAS 22574+6609 (UMB00) or Egg Nebula (e.g., Sahai et al. 1998).

3.2. DUPLEX objects

IRAS 04395+3601 (better known as AFGL 618) is a carbon-rich PPN surrounding a B0 central star, rapidly evolving to a PN stage. The ACS image shows bipolar structure of the nebula, with the extent of $15.4'' \times 4.8''$. The eastern lobe is larger ($8.25'' \times 4.75''$) and brighter ($V=15.7\text{mag}$) than western one ($6.2'' \times 3.2''$ and $V=17.1\text{mag}$). The star itself is hidden in the thick dust torus and only huge outflows are seen in the optical (Trammell & Goodrich 2002). The structure of the object is very complex. The lobes consist of shock-excited gas and dust and are composed of several jetlike structures (e.g., Sánchez Contreras, Sahai & Gil de Paz 2002). The compact HII region is present in the central part of the nebula and the circumstellar envelope contains various molecular species (e.g., Woods et al. 2003a,b).

IRAS 13428–6232 is a very faint object with no optical counterpart. The nebula is not visible in V band and parts of it are revealed in I band. The object is extended in the north-east and south-west directions with a size of more than $20''$. However, only its brightest central fragment with the size of $8.75'' \times 6.9''$ (extended perpendicularly to the whole object) is above 1σ level and could be measured. This source was studied previously by Van de Steene, van Hoof & Wood (2000), who observed a nice bipolar shape of IRAS 13428–6232 in the near-infrared with the angular size of $4.1'' \times 12.0''$ in N band and $6.0'' \times 11.0''$ in K band.

IRAS 15553–5230 is a poorly known post-AGB star. This IRAS source was observed in near-infrared by García-Lario et al. (1997) and Van de Steene, van Hoof & Wood (2000) and there was no agreement about the correct counterpart, however, Van de Steene, van Hoof & Wood (2000) noticed that the object was elongated. ISO spectrum shows no features. Our observations confirmed coordinates indicated by Van de Steene, van Hoof & Wood (2000) and revealed the bipolar shape of this small ($2.5'' \times 1.1''$) nebula. The object is very faint and the central star is invisible. The lobes differ in size and shape, which may be the effect of the nebula orientation towards observer. A small feature pointing out from the east lobe may be a faint outflow or a jet.

The extended and complex bipolar nebula of IRAS 22036+5306 was already known from the previous *HST* observations (proposal ID 9101, Sahai et al. 2003). The size of the object and magnitudes in the V and I bands determined in this paper are slightly different from the ones given by Sahai and collaborators, but the WFPC2 camera used in their observations had different plate scale and different response curve than ACS. The morphology of the object is very complex, with central ring structures, elongated lobes and faint knotty jetlike linear structures. The object is oxygen-rich, with a very characteristic feature in ISO spectra of water ice absorption at $\sim 3.1 \mu\text{m}$ (e.g., Sahai et al. 2003).

IRAS 23541+7031 (also known as M 2–56) is a PPN with a strong shock emission seen in optical line spectrum. Trammell & Goodrich (1998) discovered its bipolar nature and found weak emission extending up to $10''$ from the central bright region. From our measurements the nebula is only $3.75'' \times 1.6''$ in size in the V band and

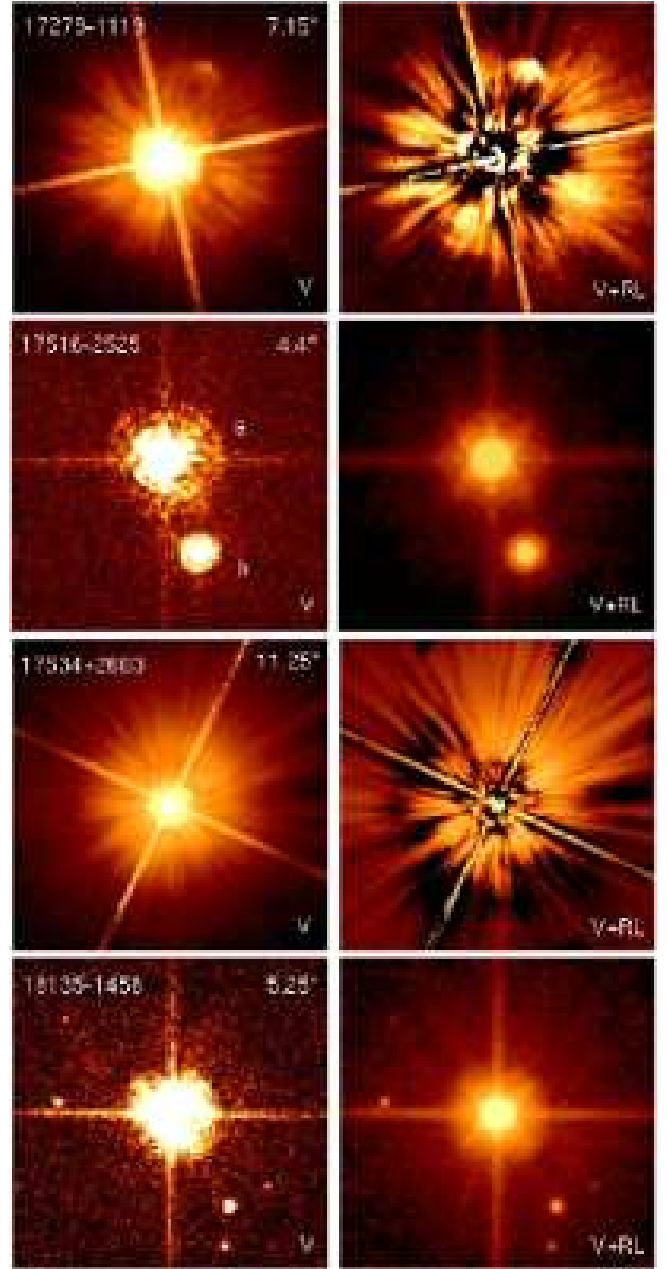


Fig.3. - Exemplary images (reduced and deconvolved) of 4 stellar objects. IRAS name, filter and size of images are shown.

smaller and much fainter in the I band. However, there is a very faint emission (below 1σ above the sky level) outside the measured size and we were not able to estimate its extent. The central star of IRAS 23541+7031, which is much fainter in the I band is classified as type B, but cooler than the central star of AFGL 618.

3.3. Stellar objects

Stellar sources are not associated with any obvious nebulosities. Objects are both very bright, like IRAS 17534+2603, and very faint, like IRAS 18135–1456. For bright sources diffraction features are very strong. Various artificial features produced during deconvolution can be seen in Figure 3.

All analyzed RV Tau stars belong to this group. They are cool post-AGB objects with effective tem-

peratures below $8000K$, usually low-mass central stars and oxygen-rich envelopes (for few exceptions see e.g., Stasińska et al. 2006) with photospheres depleted in the high condensation temperature elements as a result of gas-dust separation (e.g., Gonzalez, Lambert & Giridhar 1997). Their IR excess indicates the presence of a warm dust which should be visible as an extended circumstellar envelope. However, there is no evidence of such envelope on analyzed images. This is caused by properties of both *HST* and RV Tau stars. *HST* is sensitive to only nearby, relatively dense circumstellar dust, while RV Tau stars (because of their long-time evolution) have very extended and therefore very low surface brightness envelopes. Hence, RV Tau stars appear as stellar sources.

The rest of the objects in the stellar group are post-AGB stars with infrared excess. IRAS 12538–2611 and IRAS 15039–4806 are supergiants with cool dust, while IRAS 12222–4652 and IRAS 17279–1119 show a near-IR excess which stands for hot dust (compare SEDs on Fig.6.). It was suggested by Van Winckel, Waelkens & Waters (2000) that all objects with near-infrared excess are binaries. One of them is also IRAS 17534+2603, better known as 89 Her. It's a high-latitude F2 supergiant with a hot dust in a shell, large CO shell (Fong et al. 2006) and the $H\alpha$ line showing the evidence for the on-going mass loss (e.g., Waters et al. 1993). The model constructed for the circumstellar envelope also assumed that IRAS 17534+2603 must have evolved as a binary system. Only for IRAS 17279–1119 one can see a clump of denser material in the north-west part of an image. It must be connected with the star since there are no other objects in the near vicinity. It may be an ejected knot. The object is classified as stellar source since we do not see any evidence for continuous nebulosity around it (as it is in case of SOLE objects), but the knot makes it peculiar.

IRAS 13416–6243 was connected with a highly reddened G1 supergiant by Hu et al. (1993), but the conclusions from low resolution IRAS spectrum about 10 and $18\ \mu\text{m}$ silicate absorption bands were misleading. Instead, ISO spectrum shows moderate PAH bands and absorption feature of C_2H_2 at $13.7\ \mu\text{m}$ suggesting a carbon rich, dusty envelope. There is also a $6.9\ \mu\text{m}$ feature which is seen only in the post-AGB phase and only in objects with a $21\ \mu\text{m}$ feature (e.g., Hrivnak, Volk & Kwok 2000). Unfortunately, a $21\ \mu\text{m}$ is not seen in this object and we can only speculate that the feature is quite weak and ISO resolution was not enough to see it.

IRAS 17516–2525 is known to be an oxygen-rich source with the OH maser emission. It is a very faint star with $V \sim 17.8\text{mag}$, but analyzed images show that there are indeed 2 stars very close to each other! The separation is $1.45''$ and they are resolved only on *HST* images. It is not clear if the stars are related. IRAS 17516–2525a is redder in the *I* band than IRAS 17516–2525b and most likely this is a correct IRAS counterpart.

IRAS 20547+0247 is a peculiar variable star. IRAS 12/25 color suggests the optically thin envelope, however IRAS-LRS spectrum shows $10\ \mu\text{m}$ silicate absorption feature typical for thick dusty envelope. To explain this contradiction Barnbaum, Omont & Morris (1996) proposed a dusty, thick disk around IRAS 20547+0247 but seen edge-on. Its optical spectrum is very unusual with strong absorption and emission bands of metallic oxides, TiO,

AlO, and VO, which should be not visible in G-type star. The infrared spectroscopy revealed the hot circumstellar gas located probably in a disk-like structure (Geballe et al. 2005). We see no evidence for a disk in the images.

4. DISCUSSION

In this section we describe various properties of the analyzed objects. Table 5 compares the morphology of the objects with other properties. To get a wider view we include in our discussion other post-AGB objects observed with *HST* and already analyzed by other authors. Together there are 66 post-AGB objects with *HST* images published in the literature.

4.1. Nebulosities

The morphologies of PPNs are very complex for both SOLE and DUPLEX objects, from an optically thin nebulosities to multiple dusty outflows with microstructures as we have reviewed in §3. They are different for SOLE and DUPLEX objects, but they all show some degree of asymmetry. All nebulae are elongated. The sizes of the nebulae vary from small (e.g., $2.1'' \times 1.3''$ for IRAS 08143–4406) to big ones (e.g., IRAS 04395+3601 with the extent of $15.4'' \times 4.8''$), but the physical extension is not known due to a lack of known distances to the objects. Small or faint nebulosities can be also buried under PSF of bright central star and therefore hard to see. The surface intensity ratio between star and nebula in SOLE objects is always high, varying from 2000 to almost 340000 and the nebula appears faint in comparison to the central star. DUPLEX sources are all faint ($V=15\text{--}21\text{mag}$ in this study) and the surface intensity ratio is below 330. Hence, even huge nebulae like in AFGL 618 are not easy to detect.

As mentioned already in this paper, the observational characteristics of the nebulae are consistent with the present understanding of the structure of these shells, in which SOLE and DUPLEX nebulae respectively represent the low and high ends of the degree of equatorial enhancement for an intrinsically axisymmetric circumstellar shell. As far as the shell structure goes, there is not much of a difference between SOLE and DUPLEX nebulae, but the difference is the optical depth along the equator due to the difference in the equator-to-pole density ratio resulting from the different degree of equatorial density enhancement. Thus DUPLEX nebulae appear bipolar with a well-defined dust lane, while SOLE nebulae appear elliptical without a clear dust lane. However, their shell morphology tends to become less definitive when the optical depth along the equator is close to unity and/or the inclination angle of the shell is far from edge-on.

Table 5 shows that there is no obvious connection between morphology and characteristics of the objects in our sample. Among SOLEs we have a comparable number of carbon- and oxygen-rich objects which implies that the shapes of the nebulae are not necessary correlated with the chemical composition of the objects. Good examples are two oxygen-rich supergiants IRAS 11385–5517 and IRAS 16206–5956 and a carbon-rich AGB star AFGL 3068 (see §3.1).

Also, SOLE objects occupy a wide range of effective temperatures ($5000K < T_{\text{eff}} < 25000K$) and masses

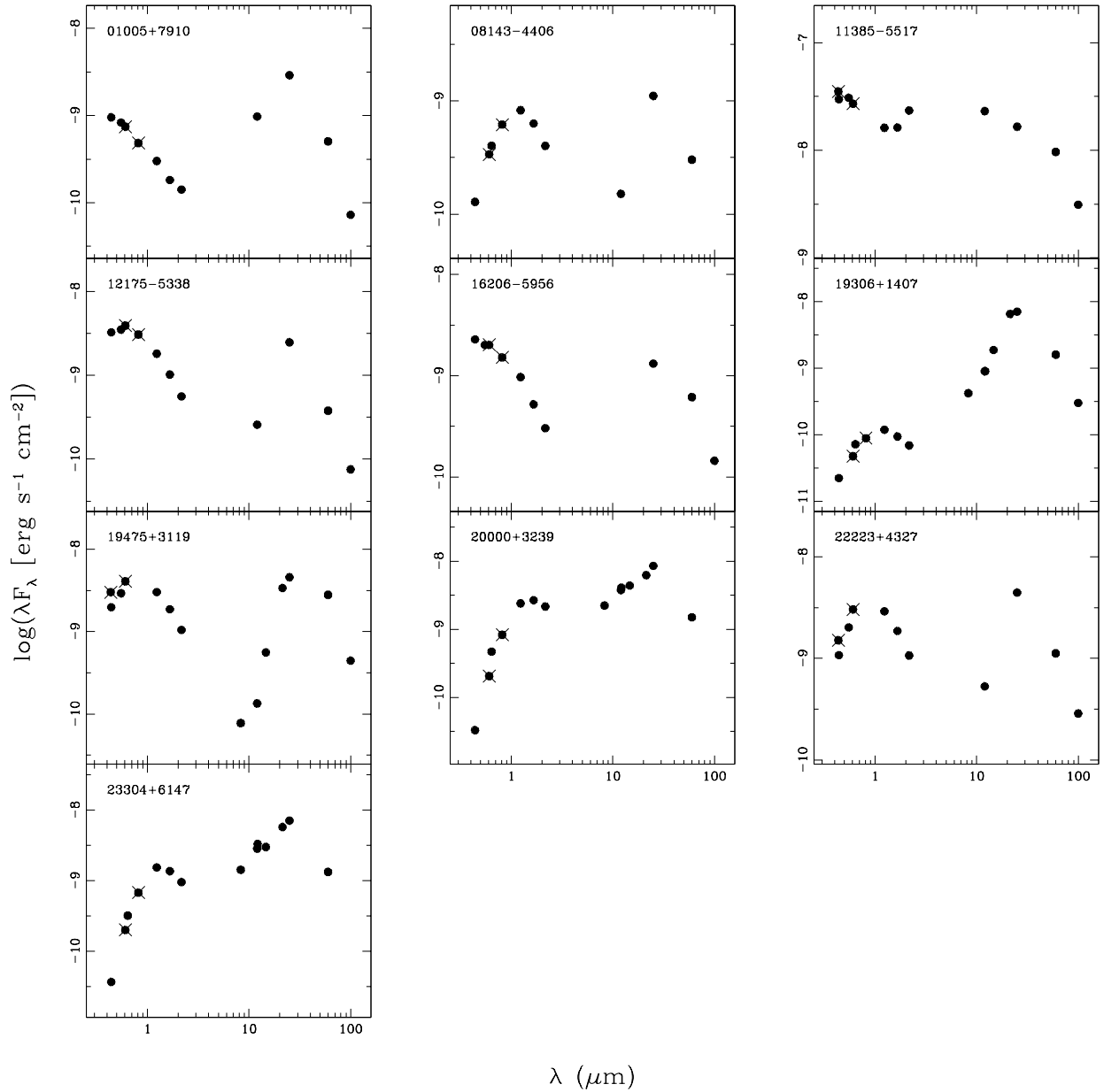


Fig.4. - Spectral energy distributions for SOLE objects shown in order of increasing RA. Values are taken from GSC2.2, 2MASS, MSX6C and IRAS catalogues. Measured HST magnitudes are shown as crossed points.

($0.55M_{\odot} < M < 0.91M_{\odot}$). Therefore, it is unlikely that SOLE morphology represents a specific evolutionary epoch and a specific mass object. The lack of known chemical composition and masses of most DUPLEXes makes it impossible to connect the morphology with these properties. The range of T_{eff} of DUPLEXes is large (K7 - B, see Table 5) and no correlation with morphology can be found. On the other hand, we find both morphologies among sources with similar chemical and physical properties, e.g. $21 \mu\text{m}$ sources: IRAS 20000+3239 and IRAS 22223+4327 are SOLEs and Egg Nebula and IRAS 06176-1036 are DUPLEXes. UMB00 also didn't find any connections between shapes of the nebulae and

properties of analyzed objects.

4.2. Magnitudes of analyzed objects

Derived B , V , and I *HST* magnitudes are in general consistent with previously published measurements, although ACS filters do not have exact counterparts in other photometric systems (photometric transformations were discussed by Sirianni et al. 2005). However, 2 DUPLEX objects, IRAS 04395+3601 and IRAS 23541+7031, are very bright in the R band in comparison to other optical wavelengths (compare also SEDs on Fig.5). AFGL 618 was not measured previously in the V band. Our measurements show it is

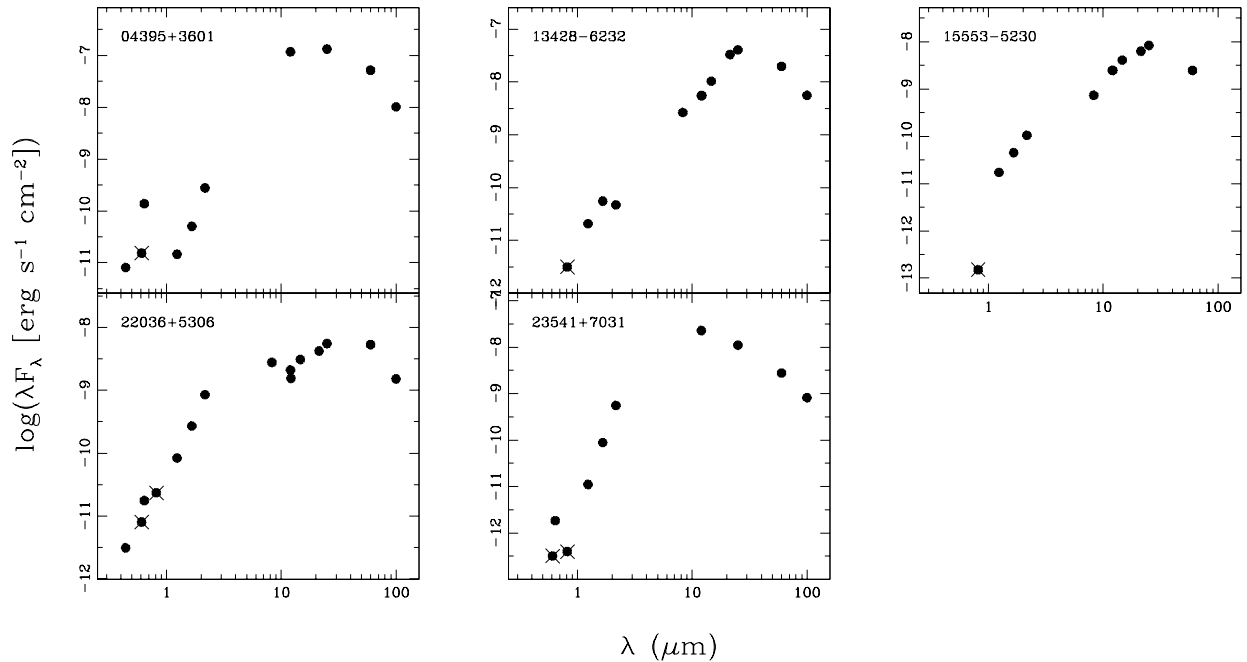


Fig.5. - Spectral energy distributions for DUPLEX objects shown in order of increasing RA. The displaying scheme is the same as in Figure 4.

faint at $V_{ACS}=15.39$. From SED (Fig.5) we see that it is also quite faint in the near-infrared. However, the object has significant line emission in $H\alpha$ (e.g., Sánchez Contreras, Sahai & Gil de Paz 2002) and that may account for the anomalous increase in the R -band brightness. Similarly, IRAS 23541+7031 is a bright source in $H\alpha$ (e.g., Trammell & Goodrich 1998) and its R magnitude is higher than expected. The $H\alpha$ line is an evidence for the ongoing mass loss and can be found in many post-AGB objects, even in RV Tau stars (e.g., Maas, Van Winckel & Lloyd Evans 2005). We do not see such a big increase of brightness in the R band in any other object in our sample.

4.3. Spectral energy distribution

Due to differences between SOLEs and DUPLEXes we expect them also to have different SED shapes, as was already discussed by UMB00. While SOLEs show both of the optical and IR peaks clearly, DUPLEXes show the prominent IR peak with a highly obscured optical peak. This is consistent with DUPLEXes being optically thicker than SOLEs due to their density distribution of a higher equator-to-pole ratio. SEDs for 33 objects which images are analyzed in this study are shown in Figures 4, 5, 6 and 7. Photometric values are taken from GSC2.2, 2MASS, MSX6C, IRAS catalogues and HST measurements. We adopted the classification scheme of van der Veen, Habing & Geballe (1989) and grouped objects into four groups: I - flat spectrum between 4 and 25 μm and a steep fall-off toward shorter wavelengths, II - maximum around 25 μm and a gradual fall-off to shorter wavelengths, III - maximum around 25 μm and a steep fall-off to shorter wavelengths with a plateau between 1

and 4 μm , IV - two distinct maxima: one around 25 μm and second between 1 and 2 μm (IVa) or below 1 μm (IVb).

In SOLE objects, the optical peak due to the central star and the infrared peak due to dust emission are clearly distinguishable. IRAS 08143-4406, IRAS 20000+3239, and IRAS 23304+6147 have the optical maximum above 1 μm and their nebulae are small (compare the sizes in Table 2) and they are of class IVa. The rest of SOLE sources, except for IRAS 19306+1407, are of class IVb with a peak below 1 μm and they have extended nebulosities. In addition, SED of IRAS 11385-5517 shows a prominent near-infrared excess that suggests a hot dust in circumstellar material and/or ongoing mass loss. SED diagram for IRAS 19306+1407 is slightly different from other SOLE objects, with a very strong cold dust emission in comparison to the stellar component, but no indication of a hot dust which could be stored in the vicinity of the central star. The size of the nebula is rather big, which is characteristic for class IVb, but the optical maximum seems to be above 1 μm like a class IVa object. It may be a case of an intermediate optical depth object with a massive circumstellar envelope that makes its dust peak higher than the stellar component. The lack of other objects with intermediate optical depth in our sample is caused by the fast evolution of post-AGB objects with effective temperature between 10000 and 16000 (e.g., Schönberner & Blöcker 1993) and hence a very small number of those objects to observe.

SEDs for DUPLEX objects are different from those for SOLE sources. The dust maximum is very prominent and the optical part is steep or flat without a clear

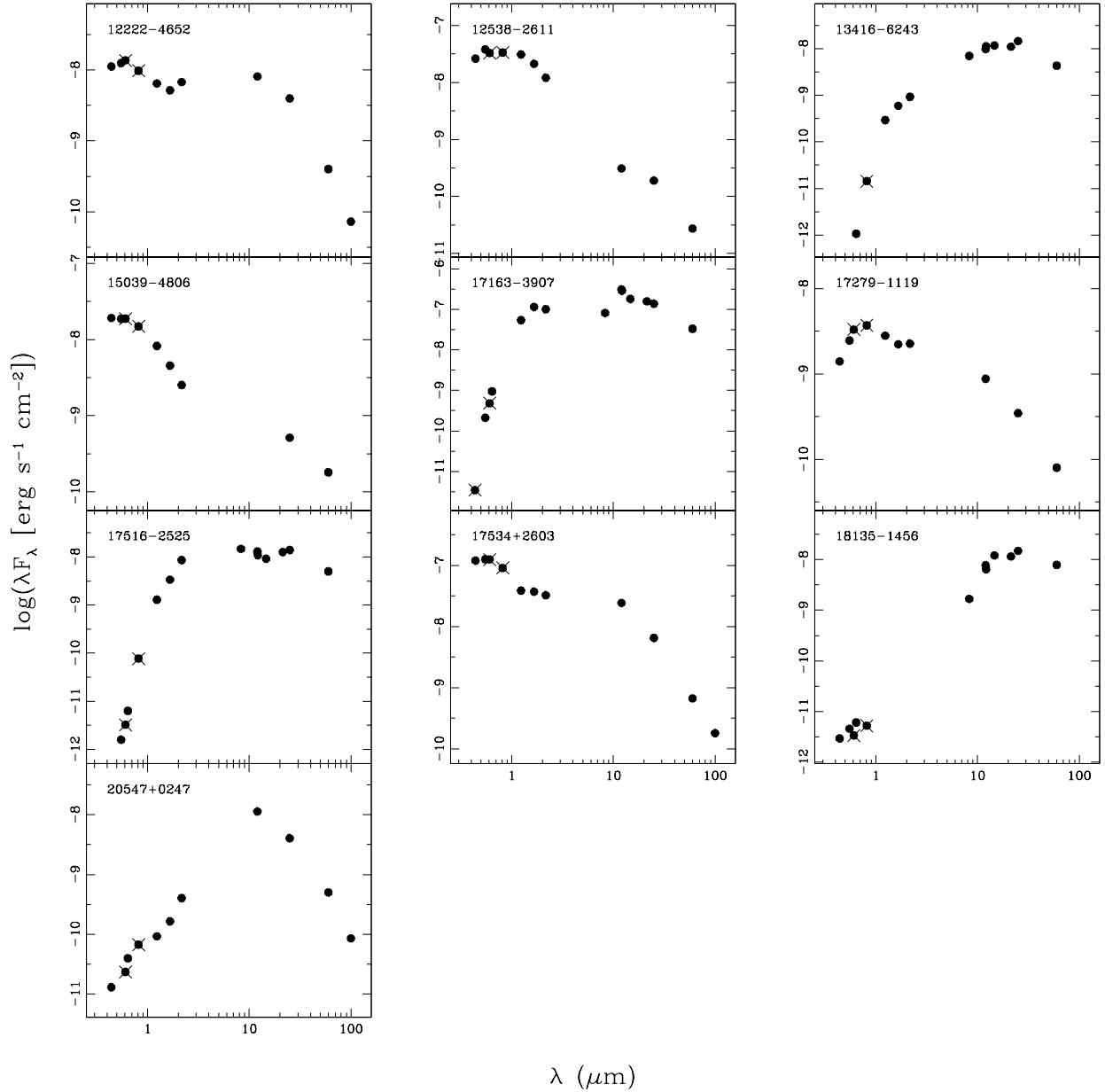


Fig.6. - Spectral energy distributions for stellar sources shown in order of increasing RA. The displaying scheme is the same as in Figure 4. SED of IRAS 18135–1456 is composed of two sources, see explanation in text, §4.3.

peak. SEDs are of class II (for IRAS 22036+5306 and IRAS 23541+7031) and III (for IRAS 04395+3601 and IRAS 13428–6232) depending on the steepness of fall-off at shorter wavelengths. We have classified IRAS 15553–5230 as type II/III.

Stellar sources show various kinds of SEDs. The non RV Tau sources can be divided into two groups. IRAS 12222–4652, IRAS 12538–2611, IRAS 17279–1119, and IRAS 17534+2603 have relatively flat optical/near-infrared spectrum decreasing in the far-infrared. One may see some resemblance of their SEDs to the SED of SOLE object IRAS 11385–5517. This indicates that these sources are actually SOLE objects without nebu-

losities, and hence, viewed pole-on and/or too distant and/or too compact for the shell to be resolved. IRAS 15039–4806 may also belong to this category, but its SED is much steeper in the mid-infrared. The second group consists of IRAS 13416–6243, IRAS 17163–3907, IRAS 17516–2525, and IRAS 20547+0247 with a steep, rising near/mid-infrared spectrum and prominent but flat far-infrared part. They look similar to SEDs of DU-PLEXes, which may suggest that they are indeed DU-PLEX sources. However, we do not see any apparent presence of circumstellar envelope/disk on *HST* images. The lack of visible nebulosities may be caused by an orientation effect as the sources with the possible tori

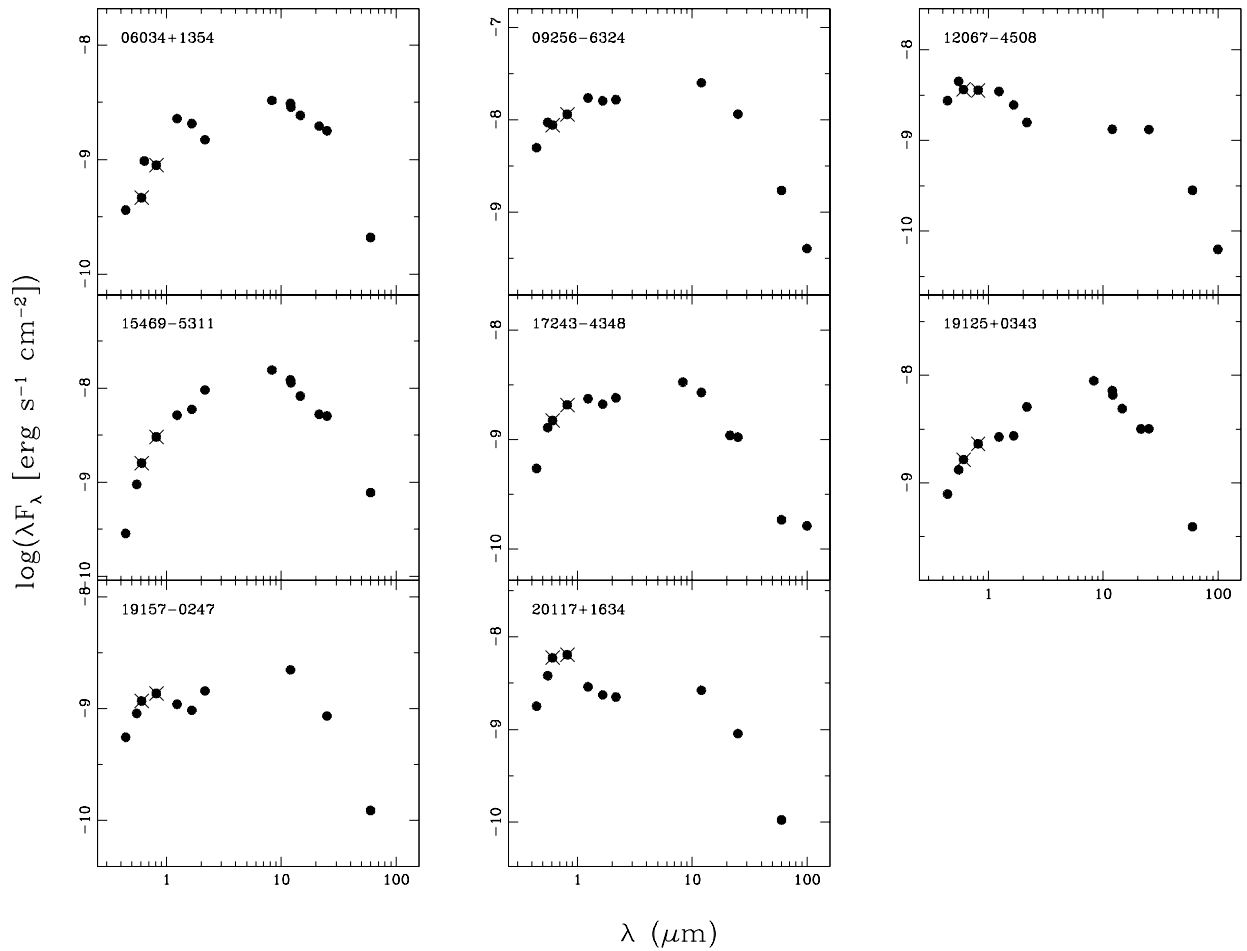


Fig.7. - Spectral energy distributions for RV Tau objects shown in order of increasing RA. The displaying scheme is the same as in Figure 4.

around are viewed almost pole-on. Dust scattering is typically anisotropic and directions of scattering almost perpendicular to the direction of incident photons are less probable (e.g., Draine 2003). Therefore, pole-on DUPLEX sources may not show obvious nebulosities. Those objects may also be too compact and/or too distant to be resolved and hence appearing as stellar sources. In fact, IRAS 13416–6243 is known to have a dusty envelope and IRAS 20547+0247 is suspected to have dusty thick disk around central star seen edge-on (see previous sections). SED of IRAS 17516–2525 is similar to the ones of DUPLEX objects, but it is constructed from the combined magnitudes of two stars unresolved up to now and the contribution from each star cannot be separated.

The SED of IRAS 18135–1458 may also appear similar to the one typical for DUPLEXes. However, while investigating this object we found that two distinct sources separated by $\sim 5''$ were identified as this object. One is weakly visible at optical wavelengths with no infrared counterpart and observed with *HST*. The other is detected only in the far-IR. The latter is most likely the correct IRAS source (also confirmed by MSX observations) and genuine post-AGB object. The SED for this object

shown in Figure 6 is then the composition of measurements of two different objects and further observation should be undertaken to characterize the optical property of this post-AGB object.

The RV Tau objects have similar SEDs with the significant infrared excess, but they cannot be classified according to the SED classification scheme of van der Veen, Habing & Geballe (1989).

4.4. Infrared color-color diagrams

Infrared data from IRAS and 2MASS catalogues allow us to construct and analyze infrared color-color diagrams. Fig.8 presents $J - K$ vs. $K - [25]$ and $J - H$ vs. $H - K$ diagrams for post-AGB objects from the paper of UMB00 and the post-AGB stars analyzed in this study. Infrared counterparts for each star were taken from the Toruń catalogue of galactic post-AGB and related objects (Szczerba et al. 2007). The transformation of 2MASS filters to Johnson system (Carpenter 2001) was done and IRAS flux at $25\mu\text{m}$ was converted to magnitude by $[25] = -2.5\log(F_\nu/6.73)$ (IRAS Explanatory Supplement 1988).

The division between different groups of objects are

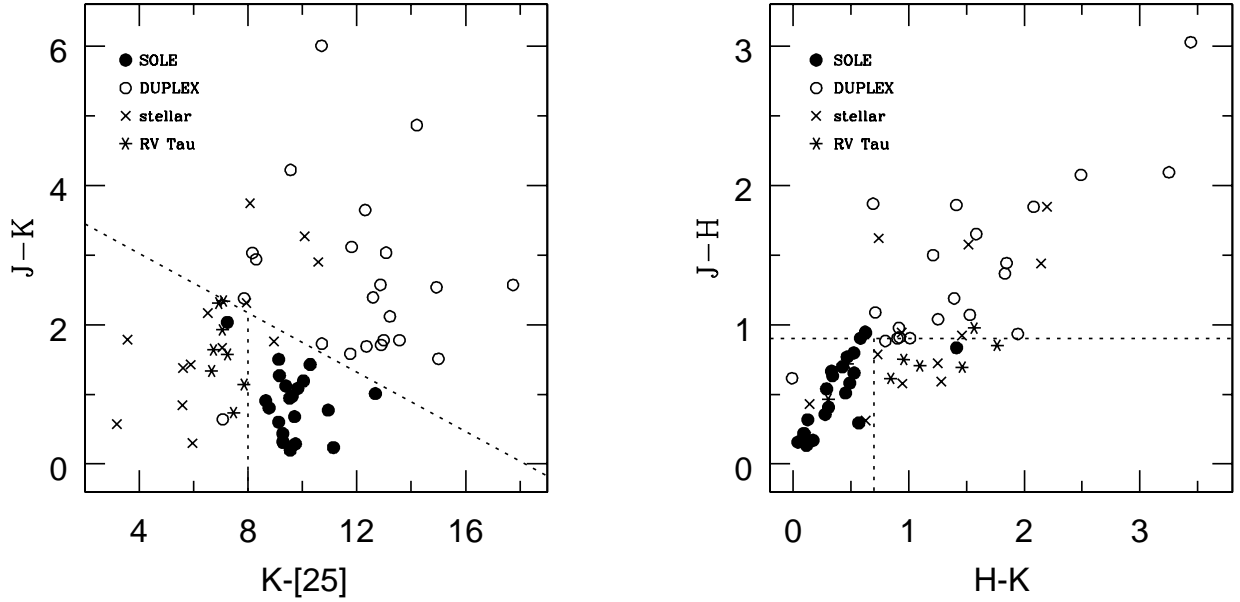


Fig.8. - Infrared color-color diagrams for post-AGB objects from Table 5. Dashed lines separate parts of the diagrams occupied by different groups of objects.

drawn in Fig.8. Clustering of SOLE, DUPLEX and stellar objects at distinct locations was already discussed by UMB00. A larger object sample in this study allowed us to draw for the first time the specific division lines. DUPLEX sources are the most red in $J - K$ color, and this is consistent with their optically thicker circumstellar shell. There is also a division of DUPLEXes around $K - [25] \sim 12$ between those with a partially visible central star ($K - [25] < 12$) and those with a fully obscured central star ($K - [25] > 12$).

SOLE objects are bluer than DUPLEXes in $J - K$ color because of a thinner dust envelope. The slightly shifted positions of IRAS 11385–5517 ($J - K = 2.0$, $K - [25] = 7.2$) is caused by the prominent near-IR excess, while the peculiar position of DUPLEX source IRAS 09371+1212 = Frosty Leo ($J - K = 0.6$, $K - [25] = 7.1$) is a result of its very bright central star and therefore unusual (for DUPLEX source) near-infrared colors.

Stellar objects are the most blue in both colors, except for few peculiar ones described in previous section. Their position on the diagram overlapping with DUPLEXes suggest they may be also DUPLEX objects, but as we discussed earlier, seen pole-on.

Also near-infrared diagram shows the differences between SOLE and DUPLEX classes. SOLE objects are bluer than DUPLEX ones in both colors, with $J - H \lesssim 1$ and $H - K \lesssim 0.7$, as it was expected for sources with clearly visible central stars and thin dust envelopes. The position of IRAS 11385–5517 ($J - H = 0.8$, $H - K = 1.4$) is caused by a presence of hot dust. Stellar objects are in general blue in $J - H$ color, $J - H \lesssim 0.9$, similar to SOLE sources, but redder in $H - K$ color, $H - K \gtrsim 0.7$, more like DUPLEX objects. It may be also a result of a hot dust very close to the star as it is in case of 89 Her. Again, 4 stellar objects discussed in section 4.2 are

found among DUPLEXes suggesting that they may be DUPLEX objects for which we did not detect the nebulae because of the orientation effect.

The differences in infrared colors between morphological classes are clearly visible and our conclusions follow and complement the results of UMB00. The study of Van de Steene, van Hoof & Wood (2000) did not recognize the IR color difference, however, there is a little overlap between their objects and ours. This is caused probably by selection. Their objects are selected based on IRAS colors. They are bright in the infrared and located close to the galactic plane, so they are biased towards more massive objects. Some of them may not be post-AGB objects, e.g., IRAS 15154–5258 is a [WR] PN.

We also analyzed IRAS color-color diagram for the objects from our study. The diagram is presented in Figure 9 and regions defined by van der Veen, Habing & Geballe (1989) are drawn. The differences between morphological classes are also clearly seen. SOLE and DUPLEX objects have similar $[12] - [25]$ colors (typical for evolved objects, located in regions IV, V and redder) but they differ in $[25] - [60]$ color with SOLEs being bluer and DUPLEXes being redder indicating colder dust in DUPLEX sources. Stellar objects are bluer in both colors and located in regions characteristic for less evolved objects (regions III and VII). Four peculiar stellar objects described in the previous sections as possibly DUPLEX sources but seen pole-on are redder in $[25] - [60]$ color than other stellar sources and located in regions VIIb and IV occupied indeed by DUPLEXes. The position of SOLE object IRAS 11385–5517 (in region VIII) is due to its cold dust. F_{12} for Frosty Leo is not certain (the quality of IRAS measurement is poor) but anyway the object is very red in $[25] - [60]$ color (2.97)

and is located outside the presented diagram. Large F_{60} excess means that the object has a detached shell composed of cold matter or a reservoir of cold matter around central star.

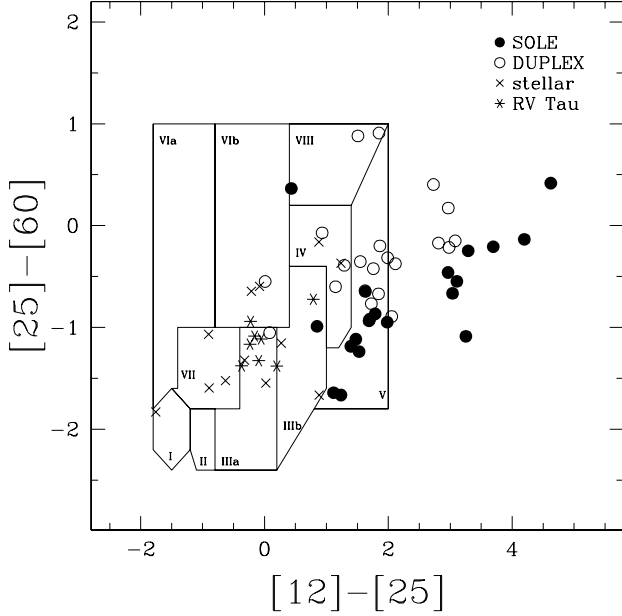


Fig.9. - IRAS color-color diagram for post-AGB objects from Table 5 with regions defined by van der Veen, Habing & Geballe (1989).

4.5. Galactic distribution

Galactic distribution of all post-AGB objects from Table 5 is shown in Fig.10. DUPLEX sources are closer to the galactic plane, while SOLEs are usually further from the galactic plane. The mean galactic latitude for DUPLEXes is $\bar{b}_{DUPLEX} = 2.35^\circ$ with the standard deviation of 10.03 (however, without peculiar Frosty Leo $\bar{b}_{DUPLEX} = 1.52^\circ$ and standard deviation is 4.92°) and for SOLEs $\bar{b}_{SOLE} = 2.58^\circ$ with the standard deviation of 11.23. Previous studies of PN (Corradi & Schwarz 1995) suggested that because of their position close to galactic plane bipolar PNs have evolved from more massive progenitors than elliptical PNs. Following those findings, UMB00 suggested that DUPLEX objects have more massive progenitors than SOLE ones and will evolve into bipolar PNs, while SOLEs will form elliptical PNs. However, the masses of DUPLEX objects and some of SOLEs are not known and this suggestion cannot be fully confirmed. The distribution of stellar objects is quite wide with the mean galactic latitude of $\bar{b}_{stellar} = 2.94^\circ$ and the standard deviation of 18.07. Some of them, like IRAS 13416–6243, lie very close to the galactic plane suggesting again that they may be in fact DUPLEX sources. On the other hand, stellar post-AGB objects far from galactic plane most likely originate from low mass progenitors and may not become PNs.

4.6. Do SOLE and DUPLEX sources have different progenitors?

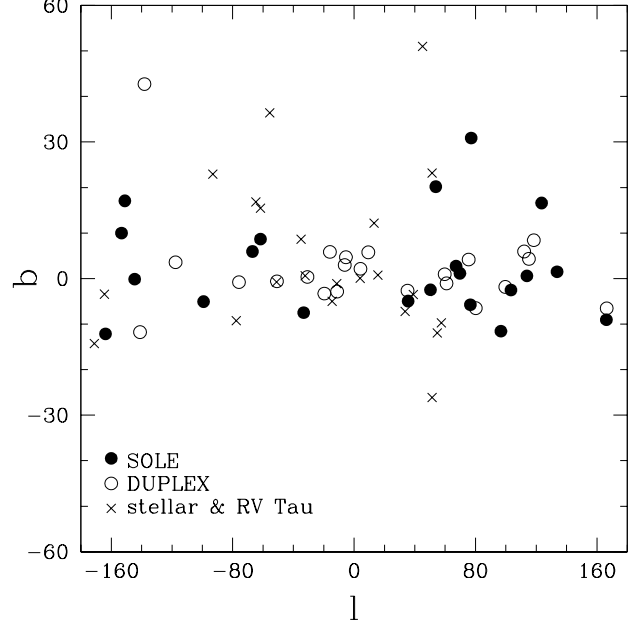


Fig.10. - Galactic distribution of post-AGB objects from Table 5.

Based on previous studies of PNs and findings from observation of PPNs, UMB00 suggested that SOLE and DUPLEX objects have different AGB progenitors with low and high masses, respectively. More massive objects will have more material in circumstellar shells and the star will be quite obscured, while it won't be in a case of object with less material in the envelope. Sources with dusty shells will therefore be fainter at the optical wavelengths but brighter in the infrared. This was already shown on color-color diagrams in Fig.8, with SOLE objects being bluer than DUPLEX ones. Knowing the masses of post-AGB objects would be the best tool to confirm this dichotomy. Derived physical parameters for 125 proto-planetary nebulae (with references) were gathered from the literature by Stasińska et al. (2006). Unfortunately, there are no information for DUPLEX objects because of the lack of optical spectra from which those parameters can be obtained. The mean mass for SOLES from this study is $\sim 0.6M_\odot$, but they can be either very massive (e.g., IRAS 17436+5003 or IRAS 07134+1005 from UMB00 with a mass of $M > 0.8M_\odot$) and very "light" (e.g., IRAS 08143–4406 from this study with a mass below $0.55M_\odot$). One has to remember also about errors on derived central star masses due to the uncertainties in effective temperature and gravity with mean values of $\Delta T_{eff} = 350K$ and $\Delta \log g = 0.3dex$ (for some objects uncertainties are large and hence a range of possible masses is big). Stellar objects in our sample are mostly of low mass, but there are some exceptions as well (e.g., IRAS 20117+1634 with a mass of $\sim 0.9M_\odot$). Figure 11 shows the distribution of masses of SOLE and stellar objects from Table 5 (masses of DUPLEXes are not known and cannot be drawn on the diagram). Masses of stellar objects are in general lower than masses of SOLEs, especially when we do not consider RV Tau stars (plain columns on the diagram).

We searched also for a connection between different morphological groups and chemistry of PPNs. In the

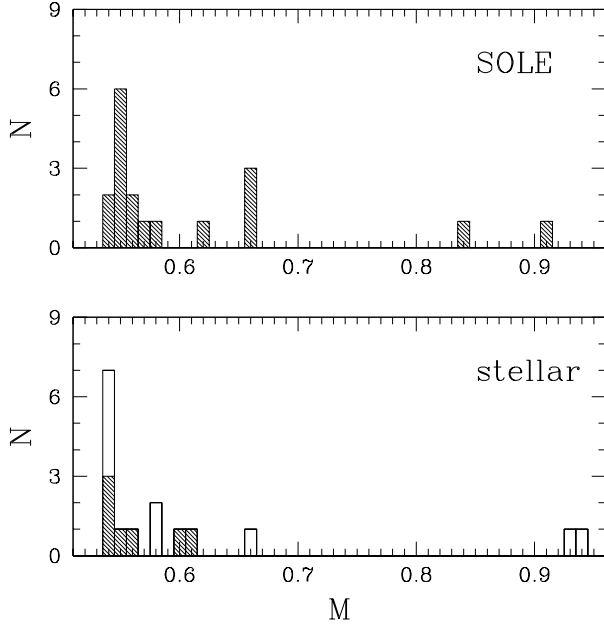


Fig.11. - Mass histogram for SOLEs and stellar objects from Table 5. The most left column shows all objects with masses below $0.55M_{\odot}$. Lower panel: plain columns correspond to RV Tau and R CrB stars.

sample of more than 50 objects from this study and UMB00 we have 12 C-rich and 9 O-rich SOLE objects and 7 C-rich and 6 O-rich DUPLEX objects. We see no obvious correlation between their chemistry and PPN morphology. However, different galactic distributions of SOLEs and DUPLEXes and therefore possibly differences in mass progenitors may suggest also the division of chemical composition. The low mass objects do not experience the 3rd dredge-up and evolve all the time as oxygen-rich sources. More massive objects experience thermal pulses and their composition undergoes significant changes, especially in carbon abundance, so they are expected to be carbon-rich. If DUPLEXes are indeed more massive they should be rather C-rich and SOLEs should be rather O-rich if they have indeed small masses. However, chemical composition depends on metallicity (e.g., Marigo, Girardi & Bressan 1999) and stars of equal masses and different metallicity can have different chemical abundances. Therefore the simple chemical division in context of masses of stars is not possible. Since we find both O- and C-rich chemistry in both SOLEs and DUPLEXes in our sample, massiveness of DUPLEXes relative to SOLEs based on the shell chemistry is not possible. However, after examining ISO, IRAS and VISIR spectra (<http://www.ncac.torun.pl/postagb> and <http://archive.eso.org/>) we do find that all DUPLEXes with the 9.8 μ m feature show it in absorption while all SOLEs with the 9.8 μ m feature show it in emission. This finding possibly indicates that DUPLEXes tend to be optically thicker than SOLEs, suggesting the more massive nature of DUPLEXes with respect to SOLEs. While it is an intriguing trend, it is nevertheless based on small number statistics (only 3 SOLE: IRAS 11385-5517, IRAS 12175-5338 and IRAS 18095+2704 and 4 DUPLEX: IRAS 08005-2356, IRAS 10197-5750, IRAS 17150-3224 and IRAS 23541+7031 objects). Thus, more

observations are needed to verify this. Most of the stellar sources in our sample is oxygen-rich (15 O-rich and 5 C-rich) and we see no correlation between their chemical composition and morphology and/or masses. Thus it cannot be said that chemistry of the central star is a key leading to differences between groups of post-AGB objects.

UMB00 found almost equal number of SOLE and DUPLEX objects, 11 and 9 respectively (the 10th DUPLEX source in their sample, IRAS 09452+1330, is an AGB star), while in our sample there are 9 SOLE and only 4 DUPLEX post-AGBs. The reason for this are selection criteria. The UMB00 sample focused mostly on sources for which evidence for spatial extension existed. Our objects were selected to complement the existing images of PPNs and to cover more diverse properties of stars. Most of them were already studied previously and hence we know their magnitudes, temperatures and chemistry. And usually they are quite bright, there are not many faint objects in our sample. This selection was also caused by requirements of snapshot survey preferring brighter stars with shorter observation time. All this provided to the lack of DUPLEX objects, which are usually very faint ($V \geq 15.4$ in our sample).

5. CONCLUSIONS

We analyzed HST images of 31 post-AGB objects. We increased the number of observed PPNs and covered a wider variety of PPNs. Following previous results of UMB00 we selected SOLE and DUPLEX sources based on their morphology. Our results are consistent with UMB00, and therefore, strengthen the validity of the general PPN structure suggested by UMB00, in which an intrinsically axisymmetric shell assumes a different morphology mainly due to the varying degree of the equatorial density enhancement which determines the presence of the dust lane in DUPLEXes and the absence of it in SOLEs. We selected a separate group of stellar post-AGB objects without visible nebulosities. We searched for connections between morphology of the nebulosities and the chemical and physical properties of their central stars and did not find any obvious connection. We confirmed results of UMB00 that SOLE objects with thin envelopes are bluer than dusty DUPLEX sources. We also suggested that some of the stellar sources may be objects with the nebulosity around central star, but seen pole-on and/or too faint and distant to be resolved. We also found the differences in galactic distribution of different groups with the SOLEs lying farther from the galactic plane than DUPLEXes, which could suggest that DUPLEX objects may have more massive progenitors. However, we were not able to confirm this suggestion directly because the masses of DUPLEXes and some SOLEs are not known.

N. Siódmiak and M. Meixner acknowledge support from NASA/NAG5-12595, NASA/STScI-GO-10627.01 and NASA/STScI-GO-09377.05. N. Siódmiak also acknowledges support from grant N203 0661 33 of the Science and High Education Ministry of Poland. T. Ueta acknowledges support from STScI GO-10627.01. R. Szczerba acknowledges support from grant N203 019 31/2874 of the Science and High Education Ministry of Poland.

REFERENCES

- Balick, B., Frank, A. 2002, *ARA&A*, 40, 439
- Barnbaum, C., Omont, A., Morris, M. 1996, *A&A*, 310, 259
- Blöcker, T. 1995, *A&A*, 299, 755
- Carpenter, J.M. 2001, *AJ*, 121, 2851
- Castro-Carrizo, A., Bujarrabal, V., Sánchez Contreras, C., Alcolea, J., Neri, R. 2002, *A&A*, 386, 633
- Cernicharo, J., Heras, A.M., Tielens, A.G.G.M., Pardo, J.R., Herpin, F., Guélin, M., Waters, L.B.F.M. 2001, *ApJ*, 546, L123
- Cohen, M., Van Winckel, H., Bond, H.E., Gull, T.R. 2004, *AJ*, 127, 2362
- Corradi, R.L.M., Schwarz, H.E. 1995, *A&A*, 293, 871
- De Ruyter, S., Van Winckel, H., Dominik, C., Waters, L.B.F.M., Dejonghe, H. 2005, *A&A*, 435, 161
- De Ruyter, S., Van Winckel, H., Maas, T., Lloyd Evans, T., Waters, L.B.F.M., Dejonghe, H. 2006, *A&A*, 448, 641
- Draine, B.T. 2003, *ApJ*, 598, 1017
- Engels, D. 2002, *A&A*, 388, 252
- Engels, D., Schmid-Burgk, J., Walmsley, C.M. 1986, *A&A*, 167, 129
- Fong, D., Meixner, M., Sutton, E.C., Zalucha, A., Welch, W.J. 2006, *ApJ*, 652, 1626
- García-Lario, P., Manchado, A., Pych, W., Pottasch, S.R. 1997, *A&AS*, 126, 479
- Gauba, G., Parthasarathy, M. 2004, *A&A*, 417, 201
- Geballe, T.R., Barnbaum, C., Noll, K.S., Morris, M. 2005, *ApJ*, 624, 983
- Gledhill, T.M. 2005, *MNRAS*, 356, 883
- Gledhill, T.M., Chrysostomou, A., Hough, J.H., Yates, J.A. 2001, *MNRAS*, 322, 321
- Gledhill, T.M., Yates, J.A. 2003, *MNRAS*, 343, 880
- Gonzaga, S. et al 2005, *ACS Instrument Handbook*, v6.0 (Baltimore: STScI)
- Gonzalez, G., Lambert, D.L., Giridhar, S. 1997, *ApJ*, 479, 427
- Hony, S., Tielens, A.G.G.M., Waters, L.B.F.M., de Koter, A. 2003, *A&A*, 402, 211
- Hrivnak, B.J., Kwok, S., Su, K.Y.L. 2000, in *ASP Conf. Ser.* 1999, *Asymmetrical Planetary Nebulae II: From Origins to Microstructures*, ed. J. H. Kastner, N. Soker & S. Rappaport (San Francisco: ASP), 155
- Hrivnak, B.J., Kwok, S., Su, K.Y.L. 2001, *AJ*, 121, 2775
- Hrivnak, B.J., Volk, K., Kwok, S. 2000, *ApJ*, 535, 275
- Hu, J.Y., Slijkhuis, S., de Jong, T., Jiang, B.W. 1993, *A&AS*, 100, 413
- Iben, I.Jr., Kaler, J.B., Truran, J.W., Renzini, A. 1983, *ApJ*, 264, 605
- Jura, M. 1986, *ApJ*, 309, 732
- Krist, J., Hook, R. 2004, *The Tiny Tim User's Guide v6.3* (Baltimore: STScI)
- Kwok, S. 1993, *ARA&A*, 31, 63
- Kwok, S., Hrivnak, B.J., Su, K.Y.L. 2000, *ApJ*, 544, L149
- Kwok, S., Volk, K., Hrivnak, B.J. 2002, *ApJ*, 573, 720
- Laidler, V. et al. 2005, *Synphot User's Guide v5.0* (Baltimore: STScI)
- Lawlor, T.M., MacDonald, J. 2003, *ApJ*, 583, 913
- Maas, T., Van Winckel, H., Lloyd Evans, T. 2005, *A&A*, 429, 297
- Maas, T., Van Winckel, H., Waelkens, C. 2002, *A&A*, 386, 504
- Marigo, P., Girardi, L., Bressan, A. 1999, *A&A*, 344, 123
- Mauron, N., Huggins, P.J. 2006, *A&A*, 452, 257
- Meixner, M. et al. 1999, *ApJS*, 122, 221
- Meixner, M., Ueta, T., Bobrowsky, M., Speck, A. 2002, *ApJ*, 571, 936
- Meixner, M., Zalucha, A., Ueta, T., Fong, D., Justtanont, K. 2004, *ApJ*, 614, 371
- Nyman, L.-Å., Hall, P.J., Olofsson, H. 1998, *A&AS*, 127, 185
- Olofsson, H. 2001, in *Science with the Atacama Large Millimeter Array*, ed. A. Wootten (San Francisco: Astronomical Society of the Pacific), 355
- Olofsson, H., Nyman, L.-Å. 1999, *A&A*, 347, 194
- Reddy, B.E., Bakker, E.J., Hrivnak, B.J. 1999, *ApJ*, 524, 831
- Reddy, B.E., Lambert, D.L., Gonzalez, G., Yong, D. 2002, *ApJ*, 564, 482
- Renzini, A. 1979, in *Stars and star systems; Proceedings of the Fourth European Regional Meeting in Astronomy* (Dordrecht, D. Reidel Publishing Co.), 155
- Reyniers, M., Van Winckel, H., Gallino, R., Straniero, O. 2004, *A&A*, 417, 269
- Sahai, R. 1999, *ApJ*, 524, 1125
- Sahai, R. 2004, in *ASP Conf. Ser.* 2004, *Asymmetrical Planetary Nebulae III: Winds, Structure and the Thunderbird*, ed. M. Meixner, J.H. Kastner, B. Balick & N. Soker (San Francisco: ASP), 141
- Sahai, R. et al. 1998, *ApJ*, 493, 301
- Sahai, R., Bujarrabal, V., Castro-Carrizo, A., Zijlstra, A. 2000, *A&A*, 360, 19
- Sahai, R., Morris, M., Sánchez Contreras, C., Claussen, M. 2007, eprint arXiv:0707.4662
- Sahai, R., Sánchez Contreras, C., Morris, M. 2005, *ApJ*, 620, 948
- Sahai, R., te Lintel Hekkert, P., Morris, M., Zijlstra, A., Likkel, L. 1999, *ApJ*, 514, L115
- Sahai, R., Young, K., Patel, N.A., Sánchez Contreras, C., Morris, M. 2006, *ApJ*, 653, 1241
- Sahai, R., Zijlstra, A., Bujarrabal, V., Te Lintel Hekkert, P. 1999, *AJ*, 117, 1408
- Sahai, R., Zijlstra, A., Sánchez Contreras, C., Morris, M. 2003, *ApJ*, 586, L81
- Sánchez Contreras, C., Sahai, R., Gil de Paz, A. 2002, *ApJ*, 578, 269
- Sarkar, G., Sahai, R. 2006, *ApJ*, 644, 1171
- Schönberner, D., Blöcker, T. 1993, in *Luminous High-Latitude Stars; The International Workshop on Luminous High-Latitude Stars*, ed. D.D. Sasselov (San Francisco: Astronomical Society of the Pacific), 337
- Sirianni, M., et al. 2005, *PASP*, 117, 1049
- Stasińska, G., Szczerba, R., Schmidt, M., Siódmiak, N. 2006, *A&A*, 450, 701
- Su, K.Y.L., Hrivnak, B.J., Kwok, S., 2001, *AJ*, 122, 1525
- Su, K.Y.L., Hrivnak, B.J., Kwok, S., Sahai, R. 2003, *AJ*, 126, 848
- Su, K.Y.L., Volk, K., Kwok, S., Hrivnak, B.J. 1998, *ApJ*, 508, 744
- Szczerba, R., Siódmiak, N., Stasińska, G., Borkowski, J. 2007, *A&A*, 469, 799
- Szczerba, R., Stasińska, G., Siódmiak, N., Górny, S.K. 2003 in *Exploiting the ISO Data Archive. Infrared Astronomy in the Internet Age*, ed. C. Gry, S. Peschke, J. Matagne, P. García-Lario, R. Lorente, & A. Salama (ESA Publications Series), 149
- Trammell, S.R. 2000, in *ASP Conf. Ser.* 1999, *Asymmetrical Planetary Nebulae II: From Origins to Microstructures*, ed. J. H. Kastner, N. Soker & S. Rappaport (San Francisco: ASP), 147
- Trammell, S.R., Goodrich, R.W. 1998, in *193rd AAS Meeting*, 1403
- Trammell, S.R., Goodrich, R.W. 2002, *ApJ*, 579, 688
- Ueta, T., Fong, D., Meixner, M. 2001, *ApJ*, 557, 117
- Ueta, T., Meixner, M., Bobrowsky, M. 2000, *ApJ*, 528, 861
- Ueta, T., Murakawa, K., Meixner, M. 2005, *AJ*, 129, 1625
- Van de Steene, G.C., van Hoof, P.A.M., Wood, P.R. 2000, *A&A*, 362, 984
- Van de Steene, G.C., van Hoof, P.A.M. 2003, *A&A*, 406, 773
- van der Veen, W.E.C.J., Habing, H.J., Geballe, T.R. 1989, *A&A*, 226, 108
- van der Veen, W.E.C.J., Habing, H.J., van Langevelde, H.J., Geballe, T.R. 1989, *A&A*, 216, L1
- Van Winckel, H. 1997, *A&A*, 319, 561
- Van Winckel, H. 2003, *ARA&A*, 41, 391
- Van Winckel, H., Reyniers, M. 2000, *A&A*, 354, 135
- Van Winckel, H., Waelkens, C., Waters, L.B.F.M. 2000, in *IAU Symposium 177, The Carbon Star Phenomenon*, ed. R.F. Wing (Kluwer Academic Publishers, Dordrecht), 285
- Van Winckel, H., Waelkens, C., Waters, L.B.F.M., Molster, F.J., Udry, S., Bakker, E.J. 1998, *A&A*, 336, L17
- Volk, K., Hrivnak, B.J., Kwok, S. 2004, *ApJ*, 616, 1181
- Volk, K., Hrivnak, B.J., Su, K.Y.L., Kwok, S. 2006, *ApJ*, 651, 294
- Volk, K., Kwok, S., Hrivnak, B.J. 1999, *ApJ*, 516, L99
- Volk, K., Kwok, S., Hrivnak, B.J., Szczerba, R. 2002, *ApJ*, 567, 412
- Waters, L.B.F.M., Trams, N.R., Waelkens, C. 1992, *A&A*, 262, L37
- Waters, L.B.F.M., Waelkens, C., Mayor, M., Trams, N.R. 1993, *A&A*, 269, 242
- Waelkens, C., Waters, L.B.M.F. 2004, in *Asymptotic Giant Branch Stars*, ed. H.J. Habing & H. Olofsson, Springer, 519
- Woods, P.M., Millar, T.J., Herbst, E., Zijlstra, A.A. 2003, *A&A*, 402, 189
- Woods, P.M., Schöier, F.L., Nyman, L.-Å., Olofsson, H. 2003, *A&A*, 402, 617

TABLE 5
MORPHOLOGY VERSUS PROPERTIES OF POST-AGB OBJECTS

IRAS ID	Prop. ID	SED type ¹	T _{eff} ²	Mass	C/O	b (deg)	References
SOLE sources							
01005+7910	10627	IVb	21000	0.55	C	16.59	13,32
Z02229+6208	6364	IVa	5500	0.56	C	1.50	13,15,16,32,38,40
04296+3429	6364	IVa	7000	0.55	C	-9.05	11,22,32,38,40,46
05341+0852	6364	IVa	6500	0.55	C	-12.14	13,16,32,38,46
06530-0213	6364	IVa	7250	0.56	C	-0.14	11,16,20,32,38,40
07134+1005	6737	IVb	7250	0.84	C	10.00	12,13,15,18,32,38,40,46
07430+1115	6364	IVa	6000	< 0.55	C	17.07	11,16,32,38
08143-4406	10627	IVa	7150	< 0.55	C	-5.07	20,32
11385-5517	9463	IVb	8500	0.55	O	5.94	19,32
12175-5338	10627	IVb	7350	0.62	O	8.66	32,45
16206-5956	10627	IVb	8500	0.66	O	-7.49	7,32
17436+5003	6737	IVb	6600	0.91	O	30.87	9,10,16,32,38
18095+2704	6364	IVa	6600	0.55	O	20.18	9,16,32,38
19114+0002	6737	IVa	6750	0.66	O	-4.96	9,32,38
19306+1407	9463	IVa	B	...	O	-2.49	13,27,48
19475+3119	9463	IVb	7750	0.58	O	2.73	9,31,32
20000+3239	9463	IVa	5500	...	C	1.16	9,13,16,47
20462+3416	6364	IVb	B1I	...	O	-5.75	9,38
22223+4327	9463	IVb	6500	0.55	C	-11.56	9,16,32,46
22272+5435	6364	IVa	5750	0.57	C	-2.52	9,32,38,39
23304+6147	9463	IVa	6750	0.66	C	0.59	16,32,46
DUPLEX sources							
04395+3601	9430	III	25000	...	C	-6.53	3,30,37
06176-1036	7297	III	7500	0.62	C/O	-11.76	4,5,16,32
08005-2356	6364	II	F5	...	C/O	3.58	16,38
09371+1212	9463	IVb	K7II	42.73	16,25
10197-5750	6816	II/III	A2I	-0.79	24
13428-6232	9463	III	C	-0.59	41
15553-5230	10627	II/III	0.36	41
16342-3814	6364	III	O	5.85	16,23
16594-4656	8210	III	B7	...	C	-3.29	34,35,40,42,49
17106-3046	8210	III	4.70	9,14,16,34
17150-3224	6364	III	G2	...	O	2.98	16,35,38
17245-3951	8210	III	-2.84	9,16,34,35
17423-1755	6364	II	B	...	O	5.78	7,38
17441-2411	6364	III	F5	...	C?	2.15	16,33,35,38
19024+0044	9463	III	-2.65	28
19374+2359	6364	II	F5	...	O	0.96	11,16,38
19477+2401	8210	II	-1.06	9,13,16,34
20028+3910	6364	III	G4	...	C	4.17	9,16,34,38,48
22036+5306	10185	II	O	-1.84	16,26,29
22574+6609	8210	II	C	5.96	16,34,38
23321+6545	6364	II/III	C	4.32	16,38
23541+7031	9463	II	B	...	O	8.42	2,18
Egg Nebula	9463	II/III	6500	> 0.94	C/O	-6.50	21,32
Stellar sources							
05113+1347	6364	IVa	5250	0.60	C	-14.29	16,32,38
10158-2844	6364	N/A	7600	0.56	C/O	22.94	5,16,32,38
12222-4652	10627	N/A	6800	< 0.55	O	-15.49	5,32,45
12538-2611	10627	N/A	6000	< 0.55	O	36.40	32,45
13416-6243	10627	II	C	-0.73	36,41
15039-4806	10627	N/A	8000	0.55	O	8.65	32,45
17163-3907	10185	II	-1.12	18
17279-1119	10627	N/A	7300	< 0.55	C	12.17	32,45
17516-2525	9463	II	O	0.06	36,44
17534+2603	10627	N/A	6550	0.61	O	23.19	5,16,32,50
18135-1456	9463	III	O	0.77	6,43
20136+1309	8210	IVa	G0	-11.97	34
20547+0247	9463	II	G	...	O	-26.11	1,8
RV Tau stars:							
06034+1354	10627	N/A	5900	< 0.55	O	-3.42	5,32
09256-6324	10627	N/A	6700	< 0.55	C	-9.24	5,32
12067-4508	10627	N/A	6000	< 0.55	O	16.82	5,32
15469-5311	10627	N/A	7500	< 0.55	O	0.63	5,32
17243-4348	10627	N/A	6750	0.94	O	-4.99	5,32
19125+0343	10627	N/A	7750	0.58	O	-3.49	5,32
19157-0247	10627	N/A	7750	0.58	O	-7.23	5,32
20117+1634	10627	N/A	5000	0.93	O	-9.76	5,32
R CrB stars:							
15465+2818	6364	N/A	6705	0.66	C	50.98	16,32,38

¹ Types of spectral energy distribution according to van der Veen, Habing & Geballe (1989). SEDs that cannot be

classified are marked as N/A.

² Spectral type is shown if T_{eff} is not known from the model atmosphere analysis.

REFERENCES: All objects are included in the Toruń catalogue of galactic post-AGB and related objects (Szczerba et al. 2007, <http://www.ncac.torun.pl/postagb>). 1. Barnbaum, Omont & Morris (1996), 2. Castro-Carrizo et al. (2002), 3. Cernicharo et al. (2001), 4. Cohen et al. (2004), 5. De Ruyter et al. (2006), 6. Engels (2002), 7. Gauba & Parthasarathy (2004), 8. Geballe et al. (2005), 9. Gledhill et al. (2001), 10. Gledhill & Yates (2003), 11. Gledhill (2005), 12. Hony et al. (2003), 13. Hrivnak, Volk & Kwok (2000), 14. Kwok et al. (2000), 15. Kwok, Volk & Hrivnak (2002), 16. Meixner et al. (1999), 17. Meixner et al. (2004), 18. Nyman, Hall, Olofsson (1998), 19. Olofsson & Nyman (1999), 20. Reyniers et al. (2004), 21. Sahai et al. (1998), 22. Sahai (1999), 23. Sahai et al. (1999), 24. Sahai et al. (1999), 25. Sahai et al. (2000), 26. Sahai et al. (2003), 27. Sahai (2004), 28. Sahai et al. (2005), 29. Sahai et al. (2006), 30. Sánchez Contreras, Sahai & Gil de Paz (2002), 31. Sarkar & Sahai (2006), 32. Stasińska et al. (2006), 33. Su et al. (1998), 34. Su et al. (2001), 35. Su et al. (2003), 36. Szczerba et al. (2003), 37. Trammell & Goodrich (2002), 38. Ueta, Meixner & Bobrowsky (2000), 39. Ueta, Fong & Meixner (2001), 40. Ueta, Murakawa & Meixner (2005), 41. Van de Steene, van Hoof & Wood (2000), 42. Van de Steene & van Hoof (2003), 43. van der Veen, Habing & Geballe (1989), 44. van der Veen et al. (1989), 45. Van Winckel (1997), 46. Van Winckel & Reyniers (2000), 47. Volk et al. (2002), 48. Volk, Hrivnak & Kwok (2004), 49. Volk et al. (2006), 50. Waters et al. (1993).